Review

Carbothermal shock enabled functional nanomaterials for energy-related applications

Wei Zhang [a],[1], Xiang Wei [a],[1], Tong Wu [c],[1], Feng Wei [b], Lianbo Ma [a], Yaohui Lv [a],[*], Weijia Zhou [c],[*], Hong Liu [c],[d],[**]

[a] School of Materials Science and Engineering, Anhui University of Technology, Maanshan 243002, Anhui, PR China
[b] School of Materials and Chemical Engineering, Chuzhou University, Chuzhou 239000, Anhui, PR China
[c] Institute for Advanced Interdisciplinary Research (iAIR), Collaborative Innovation Center of Technology and Equipment for Biological Diagnosis and Therapy in Universities of Shandong, University of Jinan, Jinan 250022, PR China
[d] State Key Laboratory of Crystal Materials, Shandong University, Jinan 250100, PR China

ARTICLE INFO

ABSTRACT

Functional nanomaterials play a pivotal role in energy fields owing to their unique properties. In recent years, the carbothermal shock (CTS) technique, as an emerging synthesis method, has shown huge potential and broad prospect in creating high-performance nanomaterials. Herein, recent progresses in the preparation of functional nanomaterials using the CTS technique are reviewed. The development history, equipment and advantages of high-temperature CTS techniques are first described. Then, the versatile nanomaterials that prepared using this method, including nanoparticles, carbon-based nanomaterials, compound nanomaterials, are thoroughly summarized. Next, the latest developments of CTS-synthesized functional nanomaterials in applications, such as catalysts, and rechargeable batteries are also presented. Finally, we present perspectives and offer research directions that can yield considerable benefits to the advancement of this promising technology.

1. Introduction

Functional nanomaterials with diverse morphologies, sizes, and compositions have shown huge potential in physical, chemical, environmental fields, etc. [1,2] Conventional synthesis methods for nanomaterials can be briefly classified into two kinds: one is "top-down", that is to say, smashed macroscopic materials using lots of techniques, and another is "bottom-up", namely, build up materials from molecules/atoms. However, these traditional methods often fail to obtain metastable nanomaterials with unique physical and chemical properties owing to their mild heating and cooling conditions [3]. Recently, some effective ultrafast synthesis strategies, such as flash Joule heating (FJH) [4], laser ablation (LA) [5–7], magnetic induction heating (MIH) [8], microwave irradiation (MW) [9], flame synthesis (FS) [10], plasma sputtering (PS) [11], carbothermal shock (CTS) [12], and others, have gained vast attentions from researchers. In comparison with traditional methods, these ultrafast synthesis strategies have offered extraordinary

kinetic processes, providing ample possibilities and brilliant prospects for synthesizing metastable materials [13–17]. In addition, these ultrafast strategies can conveniently obtain nanomaterials within extremely short timeframes (milliseconds or seconds), leading to the creation of metastable structures with noticeable deviations from thermodynamic equilibrium [12,18]. Remarkably, the atomic mobility and aggregation is strikingly hampered because of the exceedingly short heating time, bringing about the creation of inundant structural defects, such as dislocations, stacking faults, twin boundaries, Frenkel defects, and Schottky defects, among others [19–21]. These non-equilibrium characteristics intensively determine the properties of the eventual materials, such as their electrocatalytic activity, charge storage capability, and sensing response ability.

Our objective in this work is to deliver a comprehensive analysis of the latest advancements in research regarding the CTS technique for synthesizing functional nanomaterials (Fig. 1). The development history, equipment, and advantages of the CTS technique are firstly

---

* Corresponding authors.
** Corresponding author at: Institute for Advanced Interdisciplinary Research (iAIR), Collaborative Innovation Center of Technology and Equipment for Biological Diagnosis and Therapy in Universities of Shandong, University of Jinan, Jinan 250022, PR China.
E-mail addresses: yaohui@ahut.edu.cn (Y. Lv), ifc_zhouwj@ujn.edu.cn (W. Zhou), hongliu@sdu.edu.cn (H. Liu).
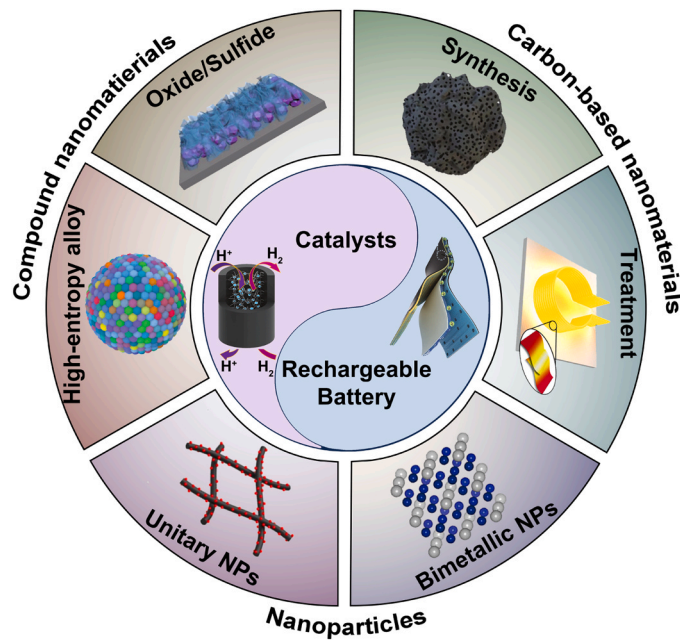[1] These authors contributed equally.

Fig. 1. Schematic diagram of the prepared functional nanomaterials using CTS technique in various fields. Reproduced with permission [22]. Copyright 2017, American Chemical Society. Reproduced with permission [23]. Copyright 2018, Wiley-VCH. Reproduced with permission [24]. Copyright 2022, American Chemical Society. Reproduced with permission [25]. Copyright 2016, American Chemical Society. Reproduced with permission [26]. Copyright 2022, Wiley-VCH. Reproduced with permission [27]. Copyright 2020, Springer. Reproduced with permission [28]. Copyright 2021, Elsevier. Reproduced with permission [29]. Copyright 2021,Wiley-VCH. Reproduced with permission [30]. Copyright 2020, Wiley-VCH.

expounded. The variety of nanomaterials prepared using the CTS technique are then comprehensively elaborated, including metal nanoparticles (NPs), carbon-based nanomaterials, and compound nanomaterials. Subsequently, the assorted applications of the above-mentioned nanomaterials are exhaustively elaborated, including their use in catalytic fields and rechargeable batteries. Finally, based on the overview of the published investigations, the outlook on the future development directions for CTS technique is also provided.

2. The CTS technique

The carbothermal shock (CTS) technique, alternatively referred to as high temperature shock (HTS), is based on the electrical Joule heating effect, which can instantaneously reach temperatures of thousands of Kelvins within milliseconds, accompanied by an extremely fast heating rate and quenching rate, rendering drastic structure changes in materials. Meanwhile, the novel and unique non-equilibrium structures are obtained by this ultrafast synthesis and processing technology, which are unattainable in conventional heating methods.

The CTS technique offers several unique advantages: (1) It allows for rapid heating and cooling rates, enabling the instantaneous decomposition of precursors owing to the high temperature and hampering transient metal aggregation thanks to the ultrafast cooling speeds. (2) The technique is capable of overcoming thermodynamic immiscibility in bimetallic systems, resulting in homogeneously non-equilibrated bimetallic NPs. (3) It can accurately tune the elemental distributions and components, microstructure and particle size by simply adjusting the parameters of CTS technique and the defect concentration of carbon-based support. (4) The instant pulse heating method can significantly reduce energy consumption, increase output efficiency, and improve productivity. Therefore, the CTS technique is incredibly popular in the energy storage and conversion fields.

2.1. Joule heating

In 1840, Joule pioneeringly described the Joule heating or Ohmic heating phenomenon, for which heat is produced when electrical current passes through conductive materials [31], and formulated the famous Joule's law ($Q = I^2Rt$, here Q is the heat quantity; I denotes the electric current; R represents the conductor's resistance; and t is the time taken). Joule heating can be classified into two ways: indirect heating and direct heating. The indirect heating approach is first to heat the resistive metal coil, subsequently, the generated heat is transferred to the precursor through radiation, convection and conduction. Although this way is convenient, it suffers from inferior power and heating rates. Conversely, the direct Joule heating method is widely popular owing to its ability that heat the target directly by passing an electric current through it. For instance, this method is commonly employed for food thawing [32], amorphous alloy transformation [33,34], ceramic sintering [35], environment purification [36], energy storage and conversion fields [37,38].

Carbon-based materials are thought to be suitable for vacuum lighting because they reduce parasitic heat losses due to higher melting and sublimation temperatures in vacuum, as well as having a higher radiant power density (0.8–0.9) than tungsten (0.4–0.5, visible wavelengths) [39,40]. Despite the fact that numerous CNT and graphene-based incandescent bulbs have been examined [41,42], they have been unable to compete with tungsten filament lamps. Here, Bao et al. [43] prepared free-standing, high-conductivity rGO-CNT nano-carbon paper via a solution-printing followed by a Joule heating strategy, which exhibited higher visible lighting efficiency than that of tungsten light bulbs (Fig. 2a-c). Moreover, this ultrapure, thin, and highly flexible rGO-CNT paper could be broadened to many other applications, such as high-temperature heaters, thermionic emission cathodes, and windshields deicing heaters.

High temperature heaters are widely employed in a range of high-temperature chemical synthesis and device processing. Via a 3D printing technique, Yao et al. [25] reported a 3D rGO-based arbitrarily shaped heater produced by a Joule heating process in viscous GO solution (Fig. 2d). The resulting printed 3D heaters featured distinctive benefits, such as high-temperature tolerance (3000 K), superfast heating and quenching rate ($\sim$ 20,000 K S^{-1}), and flexible shape and size (Fig. 2e-f).

2.2. CTS setup

Based on the Joule heating effect, two ultrafast synthesis techniques have been derived: Flash Joule heating (FJH) and Carbothermal shock (CTS). The primary difference between the two techniques is their energy sources: FJH utilizes a capacitor bank powered by high voltage discharge, while CTS relies directly on electric power sources, such as direct or alternating current. While FJH has gained numerous attentions in various fields[4,44,45], its complicated operation and use of conductive additives (such as graphene or metals) have hampered its better development. Therefore, this article focuses on the feasible and convenient CTS technique, and the equipment setup is schematically displayed in Fig. 3a. A Keithley power source provides direct current to heat the precursors on top of a glass substrate connected to copper wire with silver paste under vacuum conditions (Fig. 3b) [46]. An optical fiber spectrometer is employed to measure the emission spectrum and compute heat temperature. The recorded emission spectrum is then fitted according to the blackbody radiation equation (Eq. 1) to calculate the instantaneous temperature of the conductive precursor[43].

$$(\lambda, T) = \gamma \varepsilon_{gray} \frac{2hc^2}{\lambda^5} \frac{1}{e^{hc/\lambda k_B T} - 1} \tag{1}$$

Here k_B represents the Boltzmann constant, h represents the Planck constant, c denotes the light velocity, λ denotes the wavelength, ε_{gray} denotes the stable emissivity, and γ denotes the fitted constant. By mathematically analyzing the wavelength and spectral radiance in
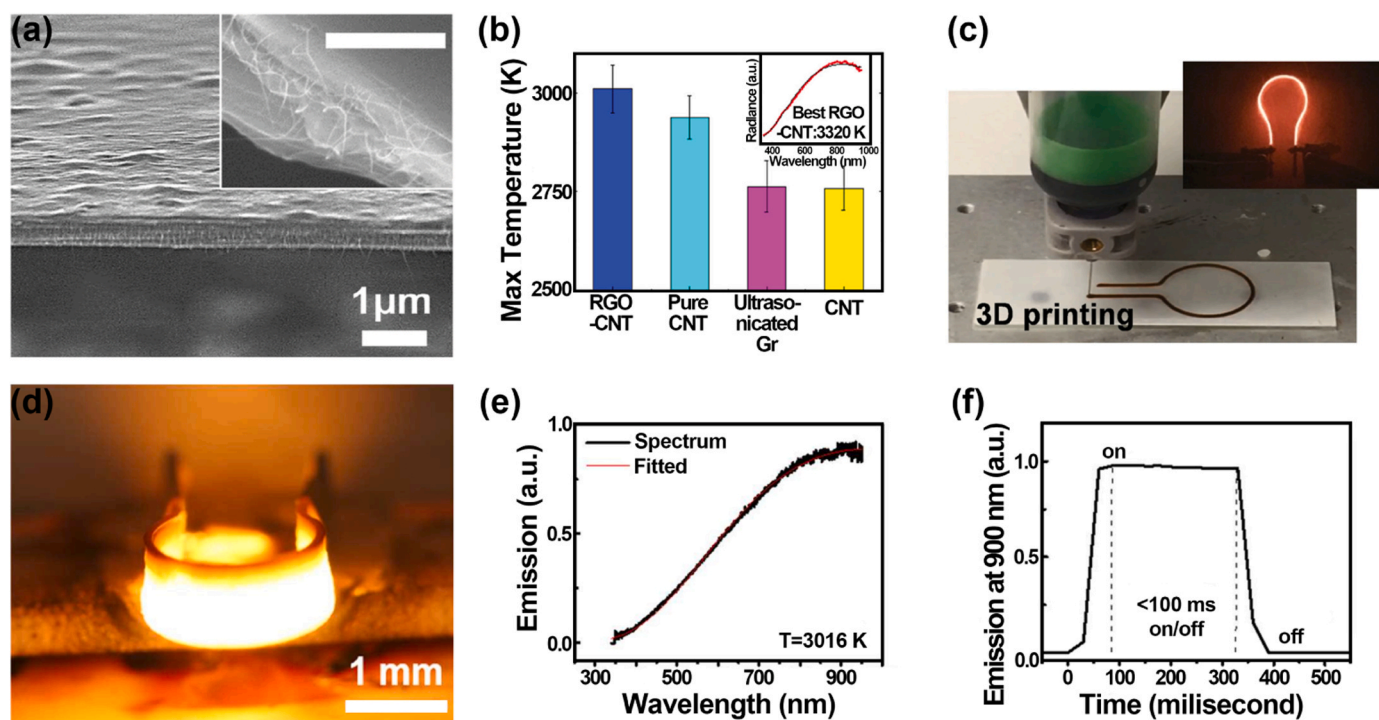
Fig. 2. (a) Cross-section SEM image of single rGO-CNT layer (thickness: about 500 nm), inset image was the edge of a torn piece. (b) The highest temperature achieved by different nanocarbon samples. Inset: the emission spectrum of the rGO-CNT sample. (c) A light bulb composed by 3D printed nanocarbon paper. Reproduced with permission [43]. Copyright 2016, Wiley-VCH. (d) Optical photo of a 3D printed graphene oxide heater. (e) The emission spectrum and fitted of rGO nanostructures at a high temperature of 3016 K. (f) The emission intensity of rGO heater was turned on and off for an ultra-short time (100 ms). Reproduced with permission [25]. Copyright 2016, American Chemical Society.

Fig. 3c, it is possible to obtain the immediate temperature of the treated precursor for a given electrical power input (Fig. 3d). In view of single-atom agglomeration and inferior compatibility with temperature-sensitive substrates, Yao and co-authors modified the original CTS method by innovatively proposing a periodic on-off heating model (Fig. 3e), involving a 55 ms on state that facilitated the formation of metal-defect bond and a 550 ms off state that stabilized single-atom and substrate [47]. In comparison with the routine CTS method, this modified method had higher demands for carbon-based support with high defect concentration and remarkable high-temperature stability. Alternatively, the periodic shockwave method was more universal, efficient and facile than the conventional CTS method. Liu et al. [48] demonstrated a rapid, continuous and scaled-up method for preparing graphene films (GF) through intensive Joule heating strategy in a roll-to-roll manner from reduced graphene oxide films (Fig. 3f). This time-efficient, energy-saving and low-cost heating method for the massive manufacture of large-area graphene (GH) films had tremendous application prospect in the flexible and wearable device fields.

Recently, Wang et al. [49] proposed traditional aerosol spray pyrolysis (SP) with CTS technique to avoid the disadvantages of SP, such as poor heating efficiency and inferior quality control. The heating element of the conventional tube furnace was superseded by a unique carbonized wood material, producing an innovative "droplet-to-particle" SP powder preparation technique. The atomized precursor droplets fly through a wood-based micro-channel reactor, and are heated to 2000 K via Joule heating in only tens of milliseconds (Fig. 3g-h). Interestingly, the support-free, homogenous and large-scale nanomaterials can be obtained by this continuous aerosol spray process. In 2021, the same research group designed a continuous fly-through high temperature apparatus using the emerging CTS technique to obtain supported NPs [50]. The reactor consisted of two face-to-face carbon paper (with a distance of 1–3 nm), which generates homogeneous and extraordinarily high temperature (~ 3200 K). Under the influence of gravity and carrier

gas, the metal salt precursors coated on carbon support flow through the heating sheets, and rapidly decompose into homogeneous NPs on a large scale (Fig. 3i). This work demonstrated a rapid, efficient and feasible strategy for synthesizing monodisperse and size controllable nanomaterials. In short, in comparison with the original heater, the modified heater has the advantages of high time-efficient, low-cost, high-throughput and continuous synthesis.

3. CTS fabrication of nanomaterials

3.1. Metals nanoparticles

An important application of CTS technique is to synthesize well-dispersed metal nanoparticles (NPs) on pre-treated conductive carbon supports, such as carbon nanofibers (CNFs) [21,22], reduced graphene oxide (rGO) film/aerosol [51,52], carbon nanotubes (CNTs) [53,54], and carbon paper/cloth/carbonized wood [55–57], utilizing microsized solid materials (such as metal, semiconductor, compound particles) or metal salt solutions as precursors. For instance, Yao et al. [22] obtained single-component palladium (Pd) NPs utilizing CTS at 2000 K for 5 ms on CNF support with $PdCl_2$ precursor solution. The size and distribution of Pd NPs were significantly impacted by the length of the thermal shock. More specifically, smaller NPs with a narrower size distribution were formed as a result of shorter thermal shock periods, as shown in Fig. 4a-b. Moreover, a non-contact and continuous "fly-through" strategy has been proposed via the rapid Joule heating radiative model to solve the knotty problem of preparing NPs on temperature-sensitive substrates (e.g., paper and textile, et al.) [58]. Apart from above-mentioned Pd NPs, various unitary metal NPs or nanoclusters, such as Sn [22], Co [51], Si [59], Ag [60], Ni [61], Cu [62], Pd [63], had also been successfully prepared using the CTS technique. Moreover, the rapid CTS technique could also be utilized to obtain bimetallic alloy NPs (e.g., PdNi [21], IrNi [53], PtFe [54], CoPd [56], NiFe [23], Pd_3Pb [24], et al.), particularly the thermodynamic immiscibility
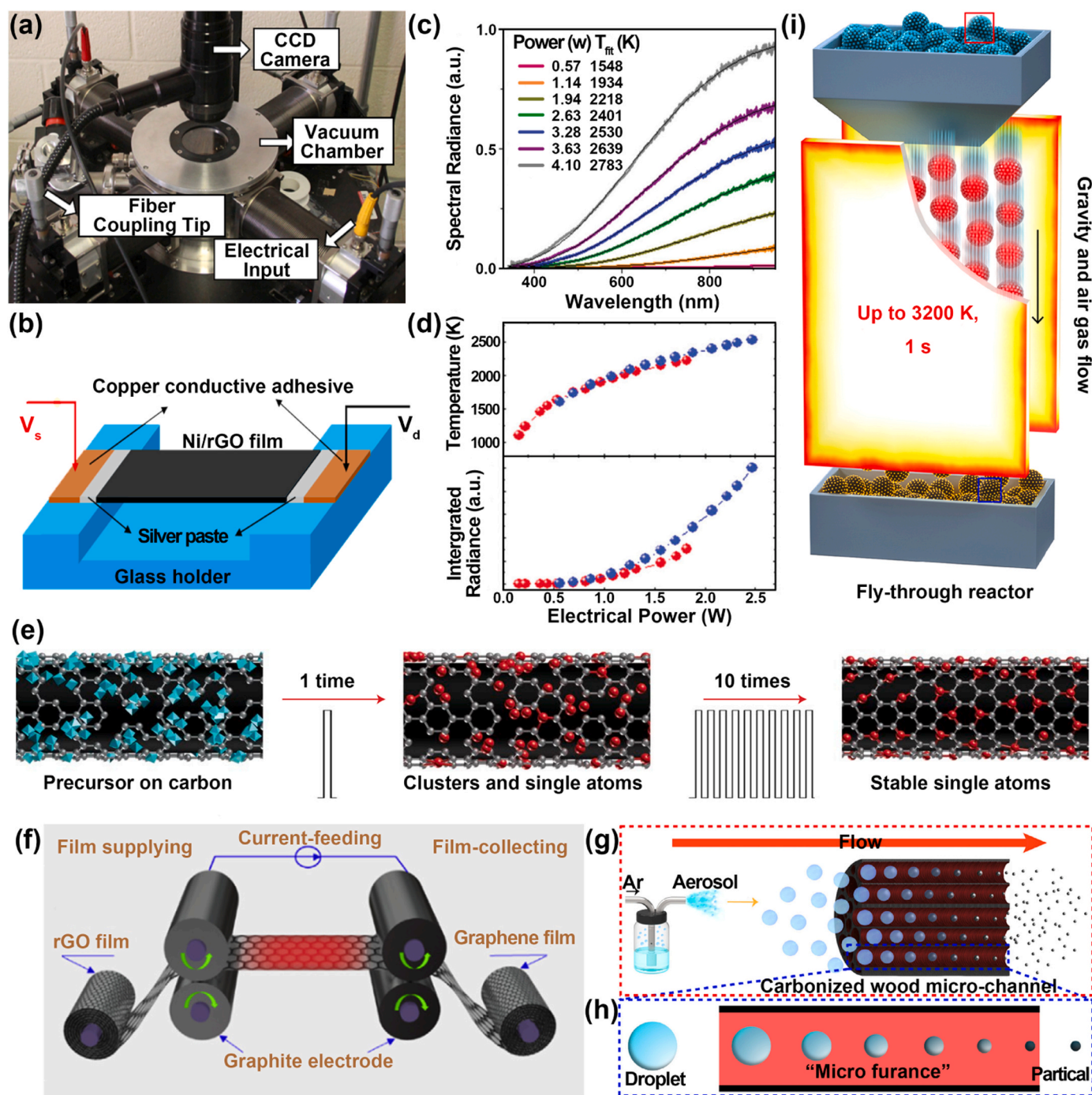
Fig. 3. (a) Photographs and (b) sketch map of self-made experiment setup for preparing materials using the CTS method. Reproduced with permission [46]. Copyright 2017, Wiley-VCH. (c) Spectral radiance measurement. Temperature is determined by Planck's law. (d) Fit temperature and integrated radiance versus input electrical power. Reproduced with permission [43]. Copyright 2016, Wiley-VCH. (e) Diagram depicting the high-temperature synthesis of single atom by precursor on carbon. Reproduced with permission [47]. Copyright 2019, Nature Publish Group. (f) Schematic of roll-to-roll Joule heating pressed graphene film. Reproduced with permission [48]. Copyright 2019, Elsevier. (g) Schematic diagram of carbonized wood microchannels transporting and heating carrier gas and liquid droplets at 2000 K (h) Diagram depicting the progression of droplets to particles in a single wood microchannel. Reproduced with permission [49]. Copyright 2020, Elsevier. (i) Schematic illustration of the fly-through high-temperature reactor. Reproduced with permission [50]. Copyright 2021, American Chemical Society.

Cu-X bimetallic systems (where X = Ag, Ni, In, Pd, Zn, and Sn) [64]. For instance, Liu et al. prepared dislocation-strained IrNi (DSIrNi) bimetallic alloy NPs on a carbon nanotube sponge via an unsteady thermal shock process in argon protective environment employing nickel chloride and iridium chloride as precursors. The HRTEM image showed that DSIrNi NPs were coated with thin carbon layers (~ 0.35 nm), which could hinder the agglomeration of IrNi NPs and improve the catalytic performance. In addition, the X-ray photoelectron spectroscopy (XPS) results also verified

that the strong electronic interaction between Ir and Ni in DSIrNi bimetallic alloy NPs. Owing to the ultrafast cooling rate and the difference in atomic radii, plentiful dislocations were kinetically embedded in IrNi NPs, inducing strain-effected high-energy surface nanostructures (Fig. 4c-f) [53]. Besides the above-discussed unitary metal NPs/nanoclusters and bimetallic alloy, high-entropy nanoalloys (e.g., PtPdCoNiFeCuAuSn [12], CoMoFeNiCu [65], PtPdRhRuIrAuCuFeCoNiZrTiHfVNb [66]) could also be prepared by carbothermal shocking mixed metal salt precursors. For
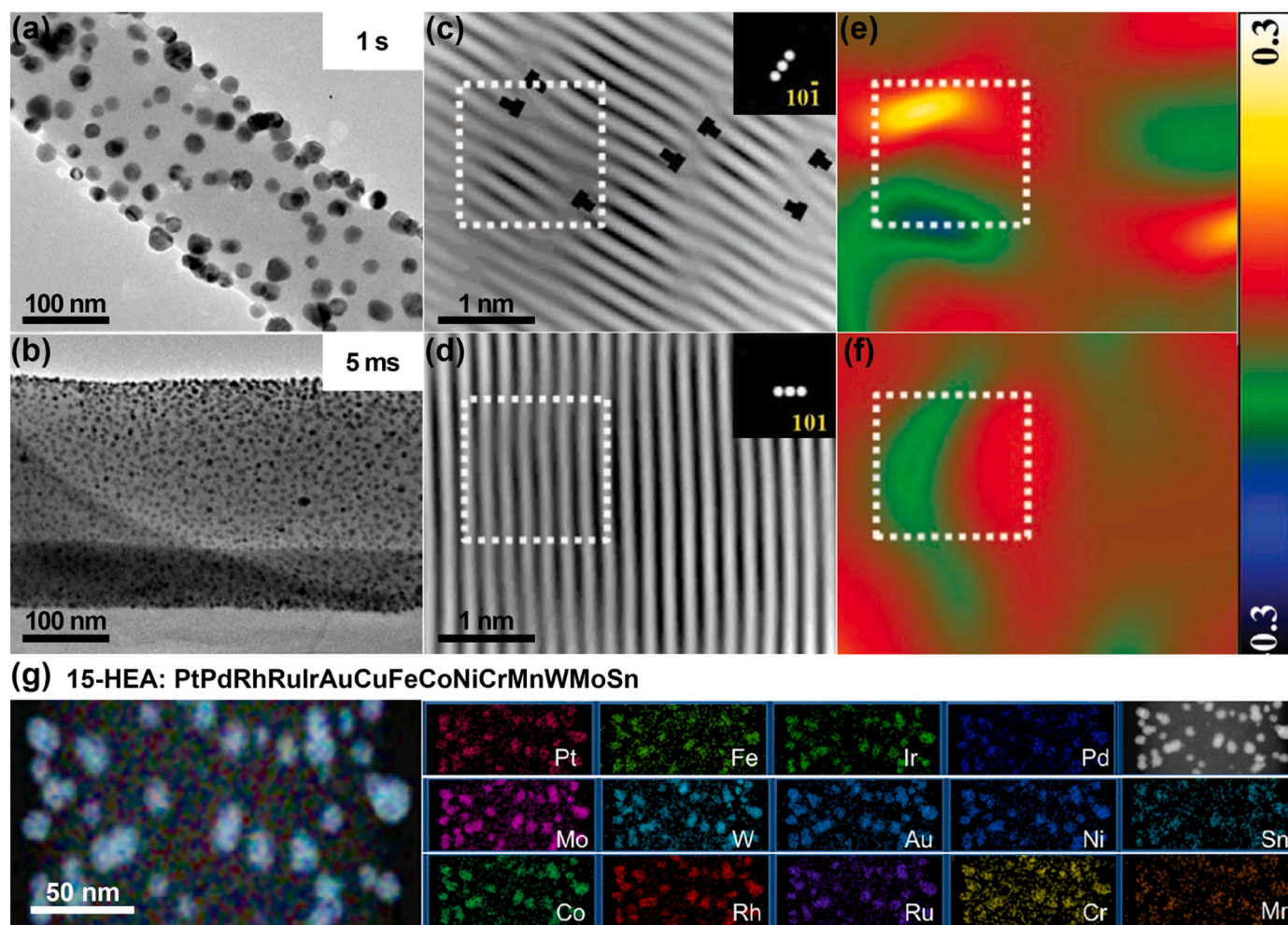
Fig. 4. TEM images of Pd nanoparticles formed on carbon nanofibers by a 1 s (a) and 5 ms (b) thermal shock treatment. Reproduced with permission [22]. Copyright 2017, American Chemical Society. (c,d) corresponding IFFT patterns along (101) and (110) crystal faces, with a substantial number of "T"-designated dislocations. (e, f) E_{xx} and E_{xy}, which stand for the (101) and (110) planes, respectively, have different distributions of strain. Reproduced with permission [53]. Copyright 2020, Wiley-VCH. (g) Large-scale element maps for 15-HEA nanoparticles showing auniform mix of early and late transition metals. Reproduced with permission [66]. Copyright 2021, Elsevier.

instance, Yao et al. pioneered the creation of a record-breaking 15-element homogeneously mixed nanoalloys through a high-temperature and high-entropy strategy (Fig. 4g)[66]. The high-temperature process avoided the reduction of nano-sized metal and reduced metal oxide impurities, while the high-entropy solid-solution structure with lattice distortions and localized strain stabilized those strongly repelling combinations and easily oxidized elements. This work tremendously widened the range of attainable nanoalloy compositions and creates a huge space for their exploitation.

3.2. Carbon nanomaterials

3.2.1. Treatment of carbon-based nanomaterials

Currently, the carbon-based nanomaterials treated by the CTS method mainly include carbon nanofibers (CNFs) [67–70], carbon nanotubes (CNTs) [71,72], and reduced graphene oxide (rGO) [25,73]. The physical-chemical properties of these materials, e.g., thermal conductivity, mechanical properties, electrical conductivity, and graphitization degree, could be considerably improved via the ultrahigh temperature treatment, leading to unrivaled and admirable performance. For instance, Yao et al. [67] obtained a 3D interconnected carbon matrix with covalent bonds by fusing adjacent polyacrylonitrile (PAN)-based CNFs under ultrahigh temperature (> 2500 K) with a super rapid heating rate (~ 200 K min^{-1}) employing Joule heating technique

(Fig. 5a-b). Compared to the pristine CNFs, the low I_D/I_G value and high peak sharpness indicated that the welded CNFs had higher crystallinity and graphitization degree (Fig. 5c). Benefiting from the high graphitization degree and covalent bond structure of the welded CNFs, the overall electrical conductivity of the integral fiber network reached nearly 380 S cm^{-1}, and the sheet resistance was 1.75 Ω sq^{-1} (Fig. 5d). These demonstrations alluded to that the high-temperature CTS technique was a fantastic strategy to transform amorphous carbon-based materials into covalently interconnected carbon networks.

3.2.2. Preparation of porous carbon nanomaterials

Biomass, which generally refers to plant-based materials derived from nature, is an excellent renewable and abundant available precursor of carbon-based materials, and has a battery of advantages of exceptional structure, richness in natural resources, biodegradability, and low price [74,75]. Developing high-performance porous carbon materials, especially graphitic carbon, from biomass is a significant topic of research. However, graphitization process is often energy-intensive and chemical-intensive owing to its high activation energy. Besides, the intrinsic defects are fatal to the electrical conductivity of graphitized carbon-based materials. Thus, Joule heating technology had been pushed into the historical stage and highly crystalline graphitic carbons derived from grass [76], lignin [77], and coconut shells [26] had been obtained. Recently, Liu et al. [26] synthesized porous carbon via
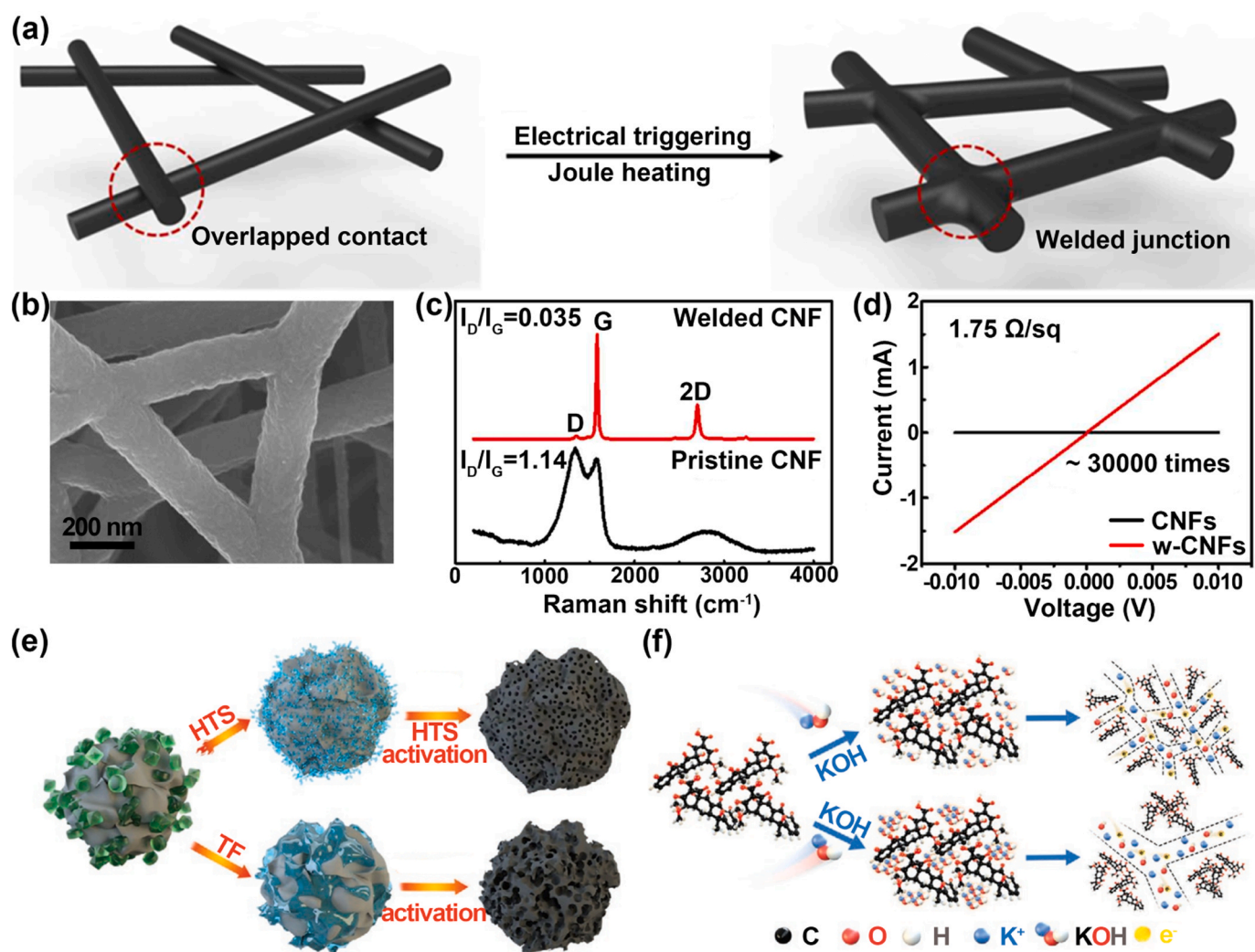
Fig. 5. (a) Diagram of the carbon welding process for CNFs by Joule heating. (b) SEM images of the welded CNF. (c) Raman spectra and (d) Conductivity was measured of the CNF film both before and after the Joule heating process. Reproduced with permission [67]. Copyright 2016, American Chemical Society. (e) Formation mechanism diagram of activated porous carbons by HTS/tubular furnace. (f) The changes of KOH aggregation pattern. Reproduced with permission [26]. Copyright 2022, Wiley-VCH.

carbonization and KOH activation strategy with high temperature CTS technique employing coconut shell as raw material. Due to the instantaneous melting of KOH into tiny droplets, which encouraged the interaction between carbon and KOH and promoted the formation of controllable, compact, and fine pores, the instantaneous Joule heating (heating rate $\approx 1100\,K\,s^{-1}$) of rapid quenching at high temperature could legitimately produce a large number of pores with uniform size distribution (Fig. 5e-f). Compared to traditional tube furnace heating patterns, the CTS technique's incomparable characteristics, including a rapid heating/cooling rate and long high-temperature holding time, made it time-saving, high efficiency, and energy-saving for preparing porous carbon. The CTS technology has the potential to revolutionize traditional methods for preparing porous carbon materials and will occupy a place in this field.

Under such fast heating/cooling conditions, many scientific and technical issues such as the removal mechanism of noncarbon species, mass transport kinetics, and the growth mechanism of graphitic carbon during carbonization and graphitization of carbon precursors are still vague. *In situ* ultrafast spectroscopy technique combined with molecular dynamic simulations maybe improve the mechanistic understanding to realize the fine tuning of the carbon microstructure.

3.3. Compound nanomaterials

In this part, the compound nanomaterials prepared via CTS technique, including carbides, oxides, phosphides, transition metal sulfides/borides, and high-entropy compounds, was introduced and discussed. (1) Carbides: Carbides have potential uses in the realm of energy conversion due to their good electrical conductivity and mechanical robustness [78]. Xie et al. [79] synthesized necklace-like SiC/C composite nanofibers employing electrospun C/Si nanofibers framework as the precursor via high-temperature CTS method (Fig. 6a). The high temperature ($\sim$ 2000 K) promoted the in-situ reaction of Si NPs and CNFs, forming uniformly distributed SiC NPs on the surface of the CNFs (Fig. 6b-c). This work simultaneously solved two critical issues, i.e., the bond strength of SiC and carbon and the homogenous dispersion of SiC NPs, in the production of SiC/C nanocomposites. (2) Oxides: Cisquella-Serra A and co-workers [80] prepared homogeneous WO_{3-x} coating on electrospun CNFs using $W(CO)_6$ as raw material via chemical vapor deposition (CVD) and Joule heating method (Fig. 6d-f). Rapid heating and quenching processes generated by the air-assisted CTS technique hampers the movement and rearrangement of steady-state atoms, thus creating rich defects and high energy state oxygen atoms, which was in favor of rapid charge transport and reaction kinetics. The
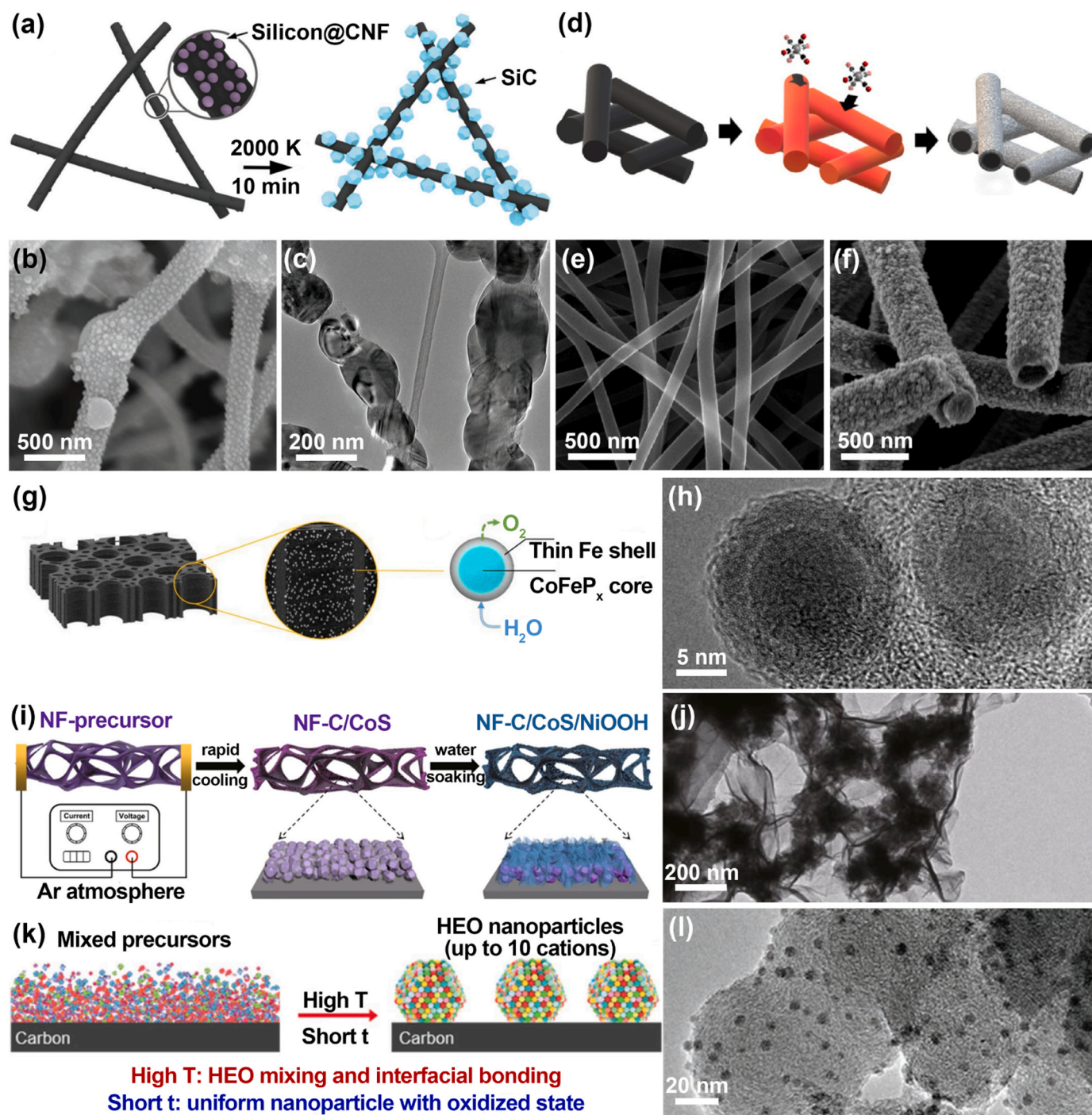
Fig. 6. (a)Schematic diagram of in situ growth of SiC/carbon nanostructure by Joule heating. (b) SEM images of the SiC nuclei formed by Joule heating treatment for 40 s (c) TEM image of the SiC/C nanostructure after ultrasonic treatment showed solid bonding between SiC and C. Reproduced with permission [79]. Copyright 2018, Wiley-VCH. (d) Schematic diagram of WO_{3-x} deposition induced by Joule heating on carbon nanofibers; SEM image of the carbon nanofibers (e) before CVD and (f) after CVD. Reproduced with permission [80]. Copyright 2022, Elsevier. (g) Hierarchy diagram of the c-wood loaded $CoFeP_x$ core-shell structures. (h) HRTEM image of the $CoFeP_x$ @Fe core-shell nanoparticles. Reproduced with permission [81]. Copyright 2019, Elsevier. (i) Preparation flow chart of NF-C/CoS/NiOOH. (j) SEM of NF-C/CoS/NiOOH. Reproduced with permission [27]. Copyright 2020, Springer. (k) Schematic diagram of the fabrication of HEO nanoparticles supported on a carbon substrate. (l) TEM image of the HEO nanoparticles. Reproduced with permission [29]. Copyright 2021, Wiley-VCH.

feasible air-assisted CTS technique had a crucial guiding significance for the realistic synthesis of other transition metal oxides. (3) Phosphides: Yang et al. [81] designed small and uniform $CoFeP_x$ @Fe nanocatalyst with core-shell structure loaded on carbonized wood by high-temperature CTS technique employing ferric nitrate, cobalt nitrate, and trioctylphosphine oxide as Fe, Co, and P sources, respectively (Fig. 6g). Owing to the vapor pressure disparity between Fe and Co

element, the $CoFeP_x$ NPs was applied with a thin layer of Fe ($\sim$ 2 nm) (Fig. 6h), protecting the surface of $CoFeP_x$ NPs from damage in the catalytic reaction process. (4) Transition metal sulfides/borides/hydroxides: Hu's research team successively reported iron disulfide (FeS_2) [52], cobalt boride (Co_2B) [82], and cobalt sulfide (CoS) [83] NPs anchored on rGO films via current-induced high temperature thermal shock technique with micro-sized FeS_2 powder, MoS_2 powder, cobalt

acetate tetrahydrate and sodium borohydride, cobalt acetate and thio-urea as the precursors, respectively. For instance, the core-shell CoS@GH NPs with a shell thickness of about 2 nm loaded on rGO nanosheets were produced via rapid CTS method (~ 7 ms) assisted by high-temperature treatment strategy [83]. The uniformly distributed CoS NPs (~ 20 nm) loaded on rGO nanosheets were caused by the ultrashort heating time and ultrafast cooling rate, which hampered the diffusion and migration of the as-obtained CoS NPs. This unique CoS@GH core-shell structure avoided the catalysts from corrosion, thus enhancing the electrocatalytic activity and stability. Recently, the NF-C/CoS/NiOOH nanomaterials-based nickel foam (NF) was designed and prepared via rapid Joule heating technique, followed by water soaking treatment [27] (Fig. 6i-j), which opened up a novel way to fabricate and manipulate NF-based nanostructured materials. (5) High-entropy compound: Hu's research group prepared a number of high-entropy compounds, such as high-entropy sulfide [84] (HEMS, i.e., $(CrMnFeCoNi)S_x$), high-entropy phosphate [28] (HEPi, i.e., CoFe-NiMnMoPi), high-entropy oxide nanoparticles [29] (HEO, i.e., (Hf, Zr, La, V, Ce, Ti, Nd, Gd, Y, Pd)O_{2-x}), and high-entropy oxide microparticles [85] (HEO, i.e., $(Mn,Fe,Co,Ni,Cu,Zn)_3O_{4-x})$, via high-temperature carbothermal reduction strategy. For instance, Li et al. [29] prepared 10-element HEO NPs (~ 7 nm) with record-high entropy homogeneously loaded on commercial carbon black substrate via the fast CTS method (≈1 s, 1400 K) employing various metal nitrates and chlorides as precursors under an air atmosphere (Fig. 6k-l). Exposing the NPs and matrix to rapid, high temperatures enhanced the interfacial binding between these materials, thereby improving the structural stability and avoiding the detachment/agglomeration of the NPs. Moreover, the high-entropy design could diminish undesirable elemental segregation, which in turn enhanced the chemical stability of the NPs. In order to obtain high-quality HEO MPs, two critical synthesis conditions must be particularly concerned: (1) It was compulsively need to fill the metal salt precursors loosely to avoid the formation of densified microstructures; (2) the heating duration demanded to be adjusted precisely to only tens of seconds.

4. Applications

4.1. Catalysts

In recent decades, heterogeneous catalysts, as a crucial component of electrochemical catalytic reactions, have gained increasing attention and industrial interest [86]. The eventual electrochemical catalytic activity is strongly determined by the particle size and distribution, as well as exposed surface area of catalytic active site. The CTS process is a feasible and effective strategy for obtaining high-efficiency electrocatalysts. Currently, the CTS technique has been extensively employed in different energy-related electrocatalytic reactions, such as the oxygen evolution reaction (OER), hydrogen evolution reaction (HER), CO_2 reduction reaction (CO_2RR), oxygen reduction reactions (ORR), N_2 reduction reaction (NRR), and ammonia (NH_3) decomposition/oxidation.
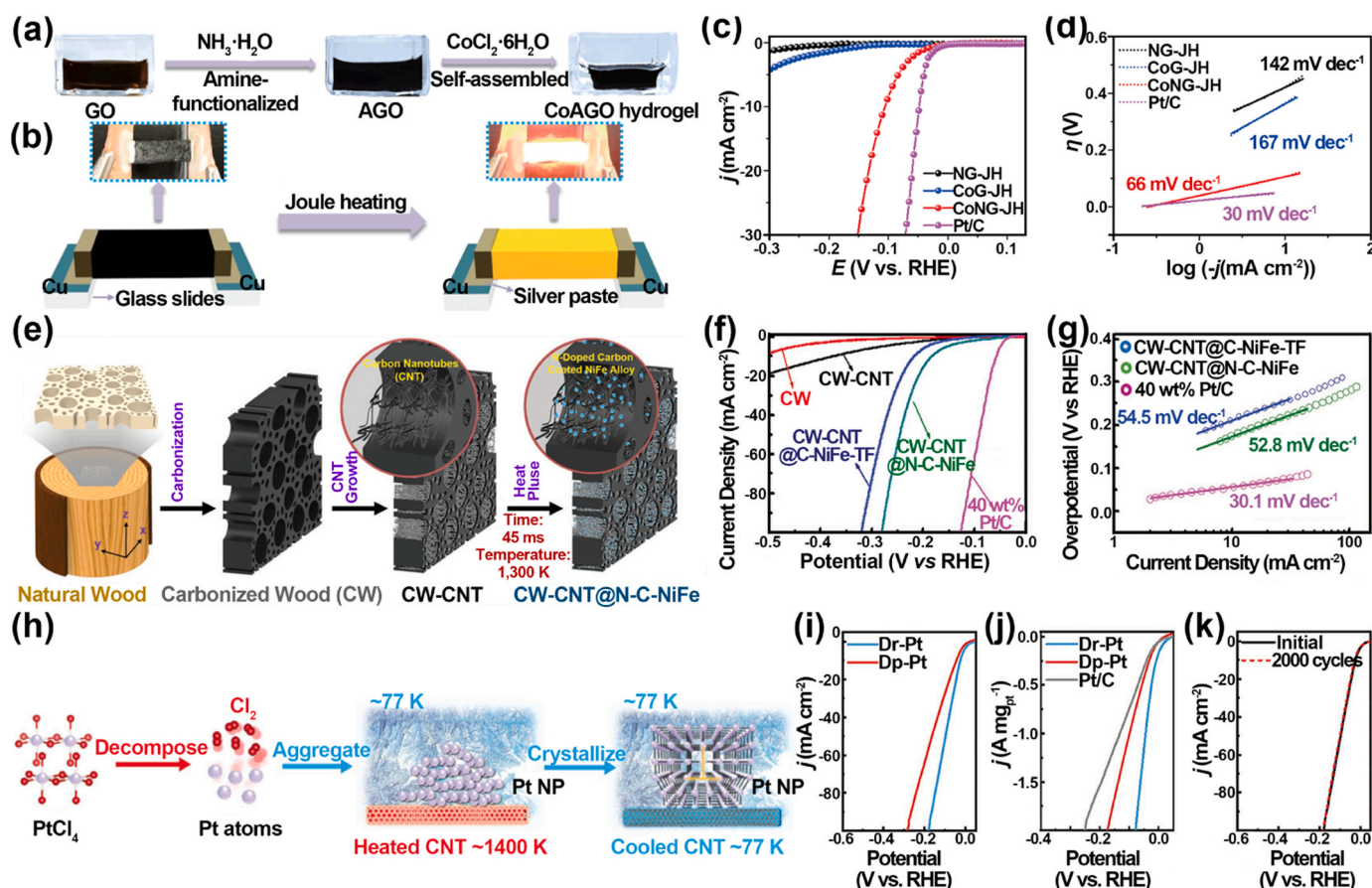

Fig. 7. (a) Schematic diagram of preparation of self-supporting CoAGO hydrogel precursor. (b) The preparation of CoAGO aerogel films by Joule heating process. (c) LSV curves and (d) Tafel slopes for CoNG-JH and contrast sample. Reproduced with permission [88]. Copyright 2022, Springer. (e) The preparation of the CW-CNT@N-C-NiFe electrode. Polarization curves (f), Tafel plots(g) of three electrodes. Reproduced with permission [23]. Copyright 2018, Wiley-VCH. (h) Environmental HTS preparation diagram for dislocation-rich Pt nanoparticles. (i) LSV curves (measured at 5 mV s^{-1}). (j) Mass activity comparison of catalysts. (k) Catalyst polarization curves measured from the first and subsequent 2000 cycles. Reproduced with permission [92]. Copyright 2022, Wiley-VCH.

4.1.1. HER

HER is a cathodic reaction of water electrolysis to obtain high-purity H_2 fuel, involving the transfer of two electrons on the catalyst surface through two separate processes, that is, the Volmer-Heyrovsky or Volmer-Tafel mechanisms [87]. The adsorption free energy of H* (ΔG_{H*}) is reference indicator used to assess HER activity, which is powerfully related to the surface geometric shape and electronic structure of the electrocatalyst. In this regard, a series of electrocatalysts have been gained using the CTS technique. Xing and co-workers [88] successfully prepared a 3D porous free-standing GH-based Co-N-C single atom (CoNG) monolith using the CTS technique (Fig. 7a-b). The fast high-temperature treating process simultaneously endowed the formation of both rGO and atomic CoN_x sites. While the ultrafast cooling rate avoided the atomic diffusion and aggregation, ensuring the homogeneous distribution of atomic CoN_x on rGO. Benefiting from the active centers of CoN_x moieties and 3D interconnected hierarchical porous architecture assembled of graphene sheets, the as-obtained self-supported CoNG electrodes delivered superior activity and durability for HER achieving 10 mA cm^{-2} at low overpotentials (106 mV) (Fig. 7c) and a small Tafel slope (66 mV dec^{-1}) (Fig. 7d) in H_2SO_4 electrolyte (0.5 M).

Due to the synergistic action of multiple metal NPs, supported bimetallic NPs are extremely important in a variety of electrocatalytic sectors to achieve increased HER activity and stability. Chen et al. recently reported chainmail electrocatalysts anchored on CNT "svilli" decorated 3D porous wood-derived frameworks, which are N-doped, few layer GH-encapsulated NiFe bimetallic NPs (N/C-NiFe) [23] (Fig. 7e). The CW-CNT's numerous, associated and low-bending microchannels can support unhindered H_2 elimination and electrolyte permeation. The ultrafine core-shell structure N/C-NiFe NPs are created using the CTS technique's rapid heating and cooling speeds. The self-supported CW-CNT@N/C-NiFe electrodes showed impressive HER activity according to these special characteristics, with a low Tafel slope (52.8 mV dec^{-1}) and an overpotential (179 mV) at 10 mA cm^{-2} (Fig. 7f-g).

The reticent kinetics of HER has been successfully addressed by strain engineering, which involves creating catalysts with defect-rich atomic structures (such as surface vacancy, doping, dislocations, grain boundary, etc.) [89–91]. Pt nanocrystals with abundant dislocations (Dr-Pt) were prepared via a high-temperature thermal-shock strategy (> 1400 K) in a liquid nitrogen cooling environment (∼ 77 K) [92] (Fig. 7h). The strain effect caused by fruitful dislocation caused by high temperature stress and corresponding structural stress during crystallization can adjust the electronic structure of Pt atom, thus regulating the adsorption energy of H_{ad} and increasing the activity of HER. In comparison with Dp-Pt (Pt NPs obtained under routine Ar atmosphere, with an overpotential of about 45 mV), Dr-Pt displayed an overpotential value as low as 25 mV (at 10 mA cm^{-2}, in 1 mol L^{-1} KOH electrolyte) (Fig. 7i). The mass activity of Dr-Pt at 50 mV overpotential was calculated to 1.16 A mg$_{Pt}^{-1}$, which was superior to that of Dp-Pt (0.42 A mg$_{Pt}^{-1}$) and commercial 20 wt% Pt/C (0.32 A mg$_{Pt}^{-1}$) (Fig. 7j). Moreover, the Dr-Pt catalysts showed negligible potential attenuation at 50 mV s^{-1} after 2000 sweeps (Fig. 7k), indicative of long-term durability. The unique extreme high-temperature environment and the fast heating/cooling rate offered a promising strategy for introducing fruitful dislocations in metal NPs for high-efficiency HER.

4.1.2. OER

In electrochemical energy storage and conversion fields such metal-air batteries and water splitting, the OER is a crucial half-cell process [93,94]. O-H bond breaking and ensuing O-O bond creation are the two primary phases in the OER process. Because of the intricate four-electron transfer mechanism and the complicated deprotonation of water or production of hydroxide during the OER process, a high overpotential is typically needed to overcome the kinetic barrier [95,96]. Due to this, it is essential to use high-efficiency electrocatalysts to lower overpotentials

and enhance OER reaction kinetics. Transition metal sulfides (M_xS_y) [84], transition metal phosphides [97–99] and HEO NPs [100] have been synthesized by the CTS technique.

For example, Cui et al. [84] pioneeringly synthesized quinary (CrMnFeCoNi)S_x HEMS NPs with uniformly dispersed and homogeneous size of 11.9 nm on a *c*-wood substrate via the CTS technique employing metal salt precursors and thiourea as the metal and S source, respectively (Fig. 8a). The (CrMnFeCoNi)S_x NPs presented striking OER activity with an extraordinarily low overpotential (295 mV at100 mA cm^{-2}), accompanying withfavorablecycling stability over 10 h at 100 mA cm^{-2} in 1 M KOH electrolyte (Fig. 8b-c). For instance, Qiao and co-workers [28] firstly reported a spherical HEPi catalysts preparedvia a high-temperature fly-through treatment of aerosol droplets (Fig. 8d). The HEPi catalyst demonstrated good OER activity in comparison to its commercial IrO_x and HEO counterparts, with overpotential and Tafel slope of 270 mV at 10 mA cm^{-2} and 74 mV dec^{-1}, respectively. These values were better than their counterparts made of commercial IrO_x (340 mV, 90 mV dec^{-1}) and HEO (350 mV, 118 mV dec^{-1}) (Fig. 8e-f). In addition, Abdelhafiz A and co-workers prepared various compositions of HEO NPs on CNFs via a rapid CTS synthesis technique in a reducing atmosphere (4% H_2 and 96% Ar gas) employing different metal salt precursors [100] (Fig. 8g). Compared to the noble IrO_2 catalyst, the senary HEO NPs (FeNiCoCrMnV) delivered higher OER activity and durability. The influence of various alloying elements (Cr, V, and Mn) on the OER catalytic activity and stability was investigated profoundly. Among the three incorporated elements, Cr had the greatest effect on the oxidation state of active elements (Fe, Ni, and Co), further presenting the best OER activity. The addition of Cr maximized the number of adsorbed high oxidation and surface oxygen species (O_2/OH$^-$) (Fig. 8h), and promoted higher oxidation state of Fe, Ni, and Co active sites. The catalyst displayed higher OER activity at the beginning, which was ascribed to the generation of smaller particles and single atom catalysts due to the dissolution of unstable elements (Mn, Cr) from the bulk to the surface (Fig. 8i). Moreover, the superior OER stability was attributed to the strong carbide-mediated intimacy, originating from the strong metal-carbide bond formed between HEO NPs and CNFs substrates.

4.1.3. ORR and CO₂RR

Depending heavily on the catalyst's surface properties, ORR either uses a direct four-electron procedure or a less effective two-electron transfer mechanism. Zeng and co-workers [54] prepared PtFe alloy NPs on defect-rich CNTs (PtFe-DCNT) via a high-temperature carbo-thermal shock treatment of the sample without a transient electro-thermal process (Fig. 9a). It was interesting that the unique preparation strategy of PtFe-DCNT material, that was, the Fe impurity NPs trapped on CNTs were delicately used as a reducing agent for Pt^{4+} ions, thus the Pt and Fe NPs on DCNT were formed. Benefiting from the unique structure, ultrafine PtFe alloy NPs (∼ 5 nm), and stabilized anchoring sites, the hybrid film electrode with low Pt content (∼ 1.7 wt%) displayed more than six times higher mass activity for ORR than the commercial 20 wt% Pt/C catalyst (Fig. 9b), superior cycling stability (90% current retention rate after 12 h) (Fig. 9c), and methanol tolerance (Fig. 9d). Additionally, the cathode of the fiber Zn-air cell shown a high discharge capacity (31.3 mA h cm^{-3}) at 10 mA cm^{-3} and improved stability thanks to the strong electrical conductivity, extraordinary mechanical resilience, and porous network structure of the PtFe-DCNT films (Fig. 9e).

Electrochemical CO₂RR is a talented method for converting CO₂ into remarkably renewable and high value-added chemicals to achieve the goals of "carbon-peak" and "carbon neutral" [101–103]. CO₂RR involves multiple proton/electron transfer processes and plenty of various surface-bound reaction intermediates, leading to sluggish reaction kinetics and inferior selectivity. The CO₂RR process can be roughly divided into three steps [104]: (1) CO₂ is adsorbed on the catalyst surface and activated to form *CO₂. (2) Protons and electrons progressively transfer to the surface-bound intermediates. (3) The surface-bound
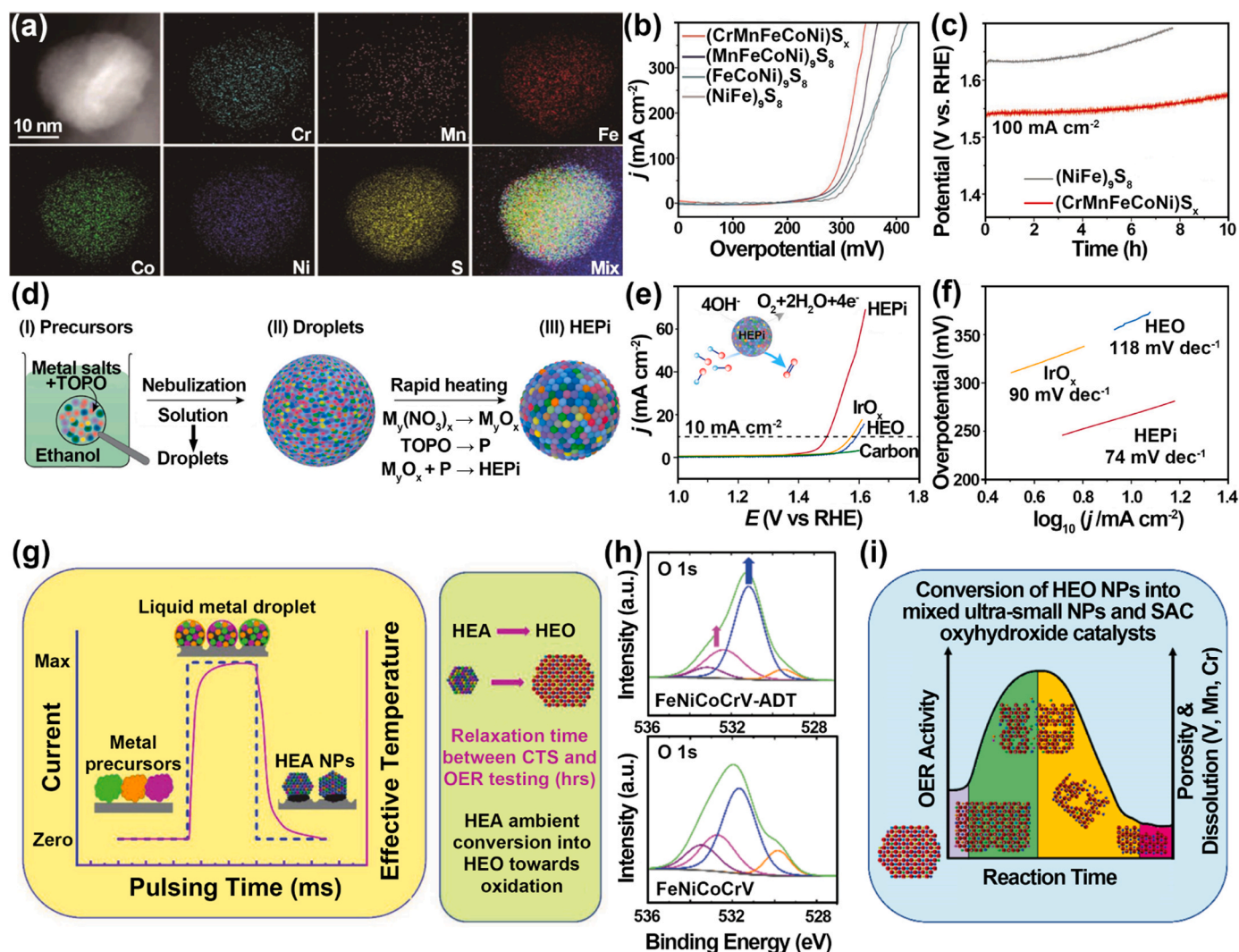
Fig. 8. (a) HAADF-STEM images and EDS mapping of a $(CrMnFeCoNi)S_x$ nanoparticle. (b) LSV curves of four samples. (c) Chronopotentiometry test of $(CrMnFeCoNi)S_x$ and $(NiFe)_9S_8$ for 10 h. Reproduced with permission [84]. Copyright 2021, Wiley-VCH. (d) Schematic of the HEPi particles formation process. (e) Polarization curves, (f) Tafel slopes in OER process between IrO_x, HEO and carbon substrates. Reproduced with permission [28]. Copyright 2021, Elsevier. (g) Diagram demonstrating the speedy Joule heating and cooling process during millisecond class pulse intervals. (h) XPS spectra of O 1 s for FeNiCoCrV before and post ADT, bottom and top, respectively. (i) The diagram depicts how the HEO structure has changed over time and how it has affected its OER performance. Reproduced with permission [100]. Copyright 2022, Wiley-VCH.

intermediates are evolved into versatile products, involving C_1 products (formaldehyde, carbon monoxide, methane, etc.) and C_2 products (propanol, acetate, ethanol, etc.). In particular, two-electron transfer can produce carbon monoxide (CO), formic acid (HCOOH), and formaldehyde (HCHO), while six- and eight-electron transfer can product ethanol (CH_3OH) and methane (CH_4). Thus, developing a CO_2RR electrocatalyst with high selectivity and activity is still imperative yet challenging.

The catalytic activity of the substance can be improved by increasing the coverage of metal NPs loaded with the carbon substrate; this is because fewer unneeded reactions will occur on the exposed carbon substrate. Song and co-workers [62] fabricated Cu NPs with a coverage ratio of $\sim$ 85% and homogeneously covered on carbonized cellulose substrate via the CTS method (Fig. 9f). The selection of partially carbonized cellulose substrate is critical to obtain a high coverage ratio of Cu NPs. With the significant binding energy of metal atoms at high temperatures, the numerous defect sites (oxygen and sp^3 bound C-C) produced during the CTS process played a crucial role in the synthesis and stability of Cu NPs. In other words, the amount of metal NPs loaded with the substrate strongly depended on the defect concentration, e.g.,

sp^3-hybridized C-C bonds, doped oxygen atoms (Fig. 9g). The as-obtained Cu NPs highly covered on cellulose/carbon paper were utilized in electrocatalytic CO_2RR, displaying 48.92% ethylene selectivity at $- 0.529\ V_{RHE}$ potential and superior stability after 30 h of reaction in 10 mol L^{-1} KOH solution (Fig. 9h-i).

The electronic structure of metal atoms is powerfully impacted by their coordination environment, which further affects the catalytic activity and selectivity [105]. Metal atoms are usually stabilized on the substrate via the coordination of non-metal elements (e.g., N, the most commonly utilized dopant) [106]. However, the majority of N dopants do not participate in the coordination with metal atoms via the formation of $M-N_x$ species. The other N species, including graphitic N, pyridine N, pyrrole N, and N-O, can induce miscellaneous negative effects on the catalyst during the catalytic reaction process. In this regard, Xi and co-workers [107] prepared Ni single-atom catalysts (SACs) on a carbon substrate with 80% N doping via the CTS strategy, employing a metal-ligand complex as the precursor (Fig. 9j). The outstanding electrocatalytic CO_2RR performance of $Ni-N_x$ SACs was ascribed to the exclusion of unwanted N species. The optimized $Ni-N_x$ SACs exhibited an excellent CO selectivity of 92% over a wide operating voltage range
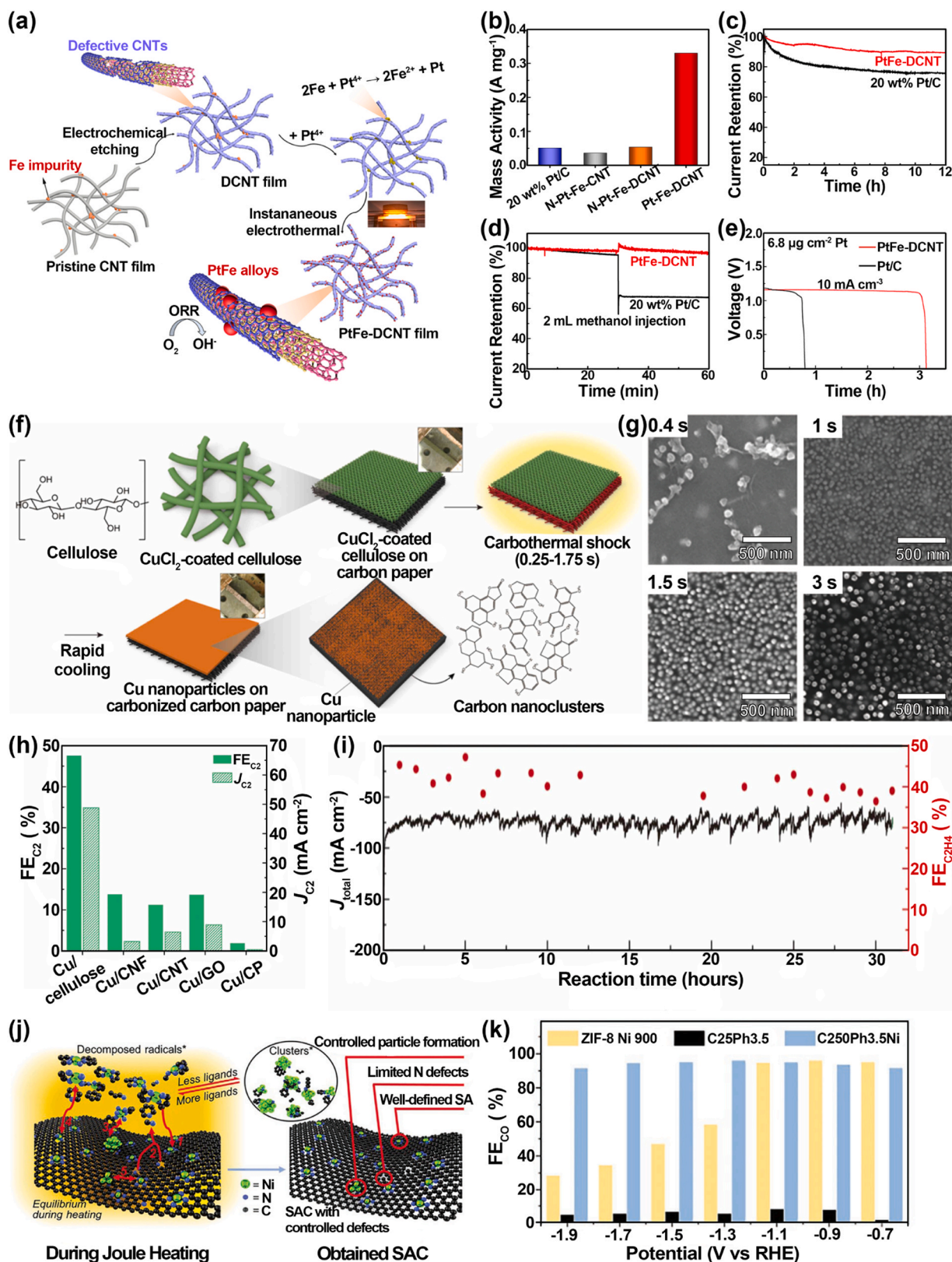
Fig. 9. (a) The preparation process of PtFe-DCNT film. (b) Mass activities, (c) stability test comparison of the catalyst films of four samples. (d) Methanol anti-poisoning of the PtFe-DCNT and 20 wt% Pt/C. (e) Discharging curves of the fiber Zn-air batteries. Reproduced with permission [54]. Copyright 2019, American Chemical Society. (f) Schematic illustration of Cu NPs on cellulose-loaded CP. (g) SEM images of Cu/cellulose/CP depending on CTS time (0.4 s ~ 3 s). (h) FE$_{C2}$ and J_{C2} on typical CTS substrates with various Cu NPs. (i) Stability test. Reproduced with permission [62]. Copyright 2021, American Association for the Advancement of Science. (j) Schematic of Joule heating processes for prepared Ni SACs. (k) Faradaic efficiency of CO with different prepared samples. Reproduced with permission [107]. Copyright 2021, Wiley-VCH.

(−0.7 to −1.9 V vs RHE) in a 0.1 mol L^{-1} KHCO$_3$ electrolyte (Fig. 9k), and unprecedented stability (activity loss < 5%) at − 1.5 V for 48 h. Noteworthily, the current density for CO could reach 70 mA cm^{-2} at a tremendously negative operating voltage (−1.9 V) in an H-cell. This impressive CTS strategy had also been employed to prepare carbon-supported Cu, Co, Zn, and Fe SACs, demonstrating its excellent universality in the preparation of carbon-supported SACs.

4.1.4. NRR and NH$_3$ decomposition/oxidation

The ambient electrocatalytic NRR method present an optional choice to the energy-intensive Haber-Bosch process for NH$_3$ production. Unfortunately, the selectivity of NRR and the formation rate of NH$_3$ are still not satisfactory owing to the competitive side reaction for HER and the tremendously strong bonding energy of N≡N in N$_2$ [108,109]. Therefore, low-cost and high-efficiency catalysts for NRR are urgently desirable. Kim and co-workers [110] prepared homogeneous RuCu alloy NPs on the cellulose/CNT sponge via the CTS method (Fig. 10a). Compared to conventional Ru-based alloy catalysts, uniform RuCu NPs delivered drastically higher selectivity (nearly 31%) and NH$_3$ formation rate (∼ 73 μg h^{-1} cm^{-2}) (Fig. 10b-c). DFT calculation results validated that the enhanced NRR activity and selectivity of RuCu alloy NPs were attributed to the more negative ΔG_{PDS} (0.75 eV) of NRR and $\Delta G(*N_2)$ -$\Delta G(*H)$ on Ru-Cu (101), which facilitated the formation of *NNH (*N$_2$ +(H$^+$+ e$^-$) →*NNH) and suppressed the adsorption of H, thus improving NH$_3$ formation rate and Faradaic efficiency.

The ammonia oxidation reaction was the key step in the industrial synthesis of nitric acid, which needed the advanced catalysts for practical application. Yao et al. [12] prepared high-entropy PtPdRhRuCe NPs anchored on CNFs substrate via the carbothermal shock metal salt mixtures precursor method. Compared with the PtPdRhRuCe MMNPs (obtained via the wet impregnation method), PtPdRhRuCe HEA-NP catalyst displayed ∼ 100% NH$_3$ conversion and > 99% selectivity to NO$_x$ (NO + NO$_2$) at 700 °C (Fig. 10d-e). Moreover, there was no obvious reduction in catalytic activity and selectivity for nearly 30 h of persistent operation at 700 °C (Fig. 10f), which was ascribed to the high entropy characteristic of the catalysts obtained via the CTS approach. For instance, Xie et al. [65] fabricated high entropy CoMoFeNiCu NPs with homogeneous elemental distribution and immiscible tunable Co/Mo element ratio via feasible CTS technology (Fig. 10g). In comparison with conventional bi-metallic Co-Mo and mono-metallic Ru catalysts, the high-entropy alloy (HEA) demonstrates significantly promoted the catalytic performance and durability for NH$_3$ decomposition. The catalytic performance of HEA NPs strongly depends on the Co/Mo atomic ratios (Fig. 10h). The mass yield of 22.1 g_{NH3} g_{metals}^{-1} h^{-1} at 500 °C for HEA-Co$_{25}$Mo$_{45}$ catalysts was achieved, which was almost 19 times higher than that of conventional Co-Mo catalysts (Fig. 10i). Moreover, there was negligible degradation in catalytic activity during continuous operation for nearly 50 h at 500 °C (Fig. 10j), demonstrating fantastic catalytic cycling stability.

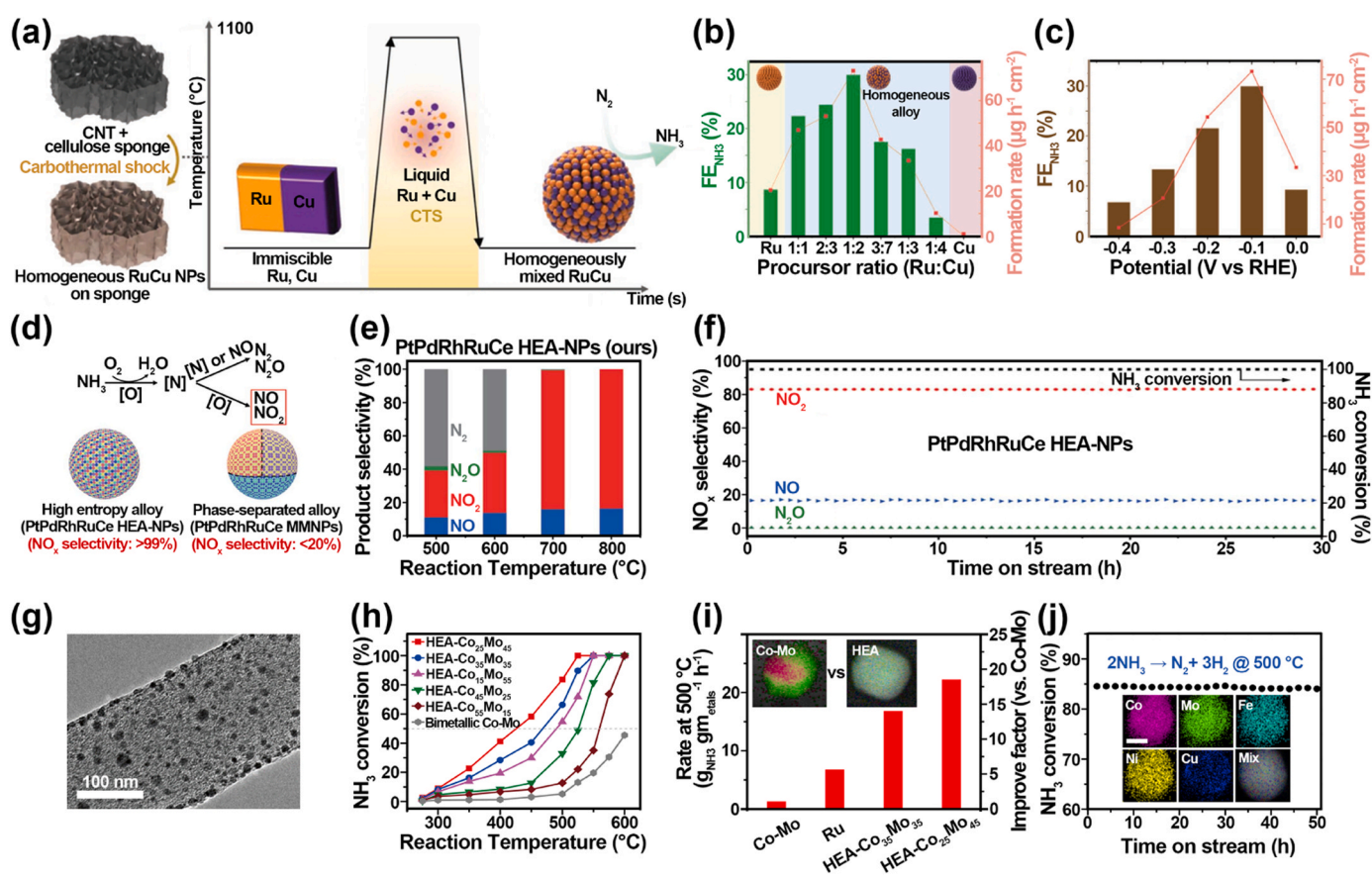The unique catalysts with non-equilibrium and metastable structures

Fig. 10. (a)The production and structure of RuCu nanoparticles on the cellulose/CNT sponge. (b) NH$_3$ yields and FE$_{NH3}$ with different ratio of Ru/Cu precursor. (c) NH$_3$ yields and FE$_{NH3}$ with different applied potentials of RuCu NPs. Reproduced with permission [110]. Copyright 2022, Wiley-VCH. (d) Process flow chart for the oxidation of ammonia and the difference in structure and properties between HEA-NPs prepared by wet impregnation and control samples. (e) PtPdRhRuCe HEA-NPs' temperature-dependent product dispersion and NH$_3$ conversion. (f) The stability test of PtPdRhRuCe HEA-NPs at 700 °C. Reproduced with permission [12]. Copyright 2021, American Association for the Advancement of Science. (g) TEM images of the HEA nanoparticles showed well dispersed on CNFs. (h) NH$_3$ conversions with different HEA-Co$_x$Mo$_y$ nanoparticles and bimetallic Co-Mo. (i) Different catalysts' speeds of reactions at 500 °C (as measured in the kinetic regime). The bimetallic Co-Mo and HEA-Co$_{25}$Mo$_{45}$ catalysts' element maps are shown in the inset. (j) The catalyst for HEA- Co$_{25}$Mo$_{45}$ underwent a stability test. After the stability test, the catalyst's elemental map is included. Reproduced with permission [65]. Copyright 2019, Nature Publish Group.

produced by the CTS technique are under booming development due to their eminent electrocatalytic activity. Nevertheless, the profound understanding the forming mechanism of these unique structures remains mostly vague. In addition, how to precise control the catalyst structure and whether the metastable structure remains stable during the electrocatalytic process are all outstanding and challenging questions.

4.2. Rechargeable batteries

With the ever-increasing energy consumption and environmental deterioration, electrochemical energy storage (EES) devices have gained numerous attentions due to their cost-effectiveness, environmental friendliness, high dependability, and satisfactory energy and power density [111,112]. Thus, rechargeable batteries have been under booming development in recent years. In this section, the modification of current collectors and the solid electrolytes using the CTS technology,

Li-ions batteries and Li-air batteries are introduced [26,113].

4.2.1. Current collectors and electrolyte

The current collector, which is a fundamental component of rechargeable battery, plays a vital role in interface stabilityand electrochemical performance. The lightweight and highly conductive current collectors, such as CNT films, rGO films, and flexible graphite foils, show great potential owing to the notorious drawbacks of routine metal-based current collectors (such as Ti, Ni, stainless steel, etc.), which are heavy, high cost, bulky, and apt to corrosion over prolonged use. However, the inferior conductivity and high cost of these carbon-based films do not meet the practical requirement of batteries. Therefore, creating flexible, lightweight current collectors that are highly conductive is crucial for the creation of high-performance rechargeable batteries. For instance, Chen and co-workers [73] fabricated rGO films with high conductivity ($3112 \, S \, cm^{-1}$), thin thickness ($\sim 4 \, \mu m$) and small
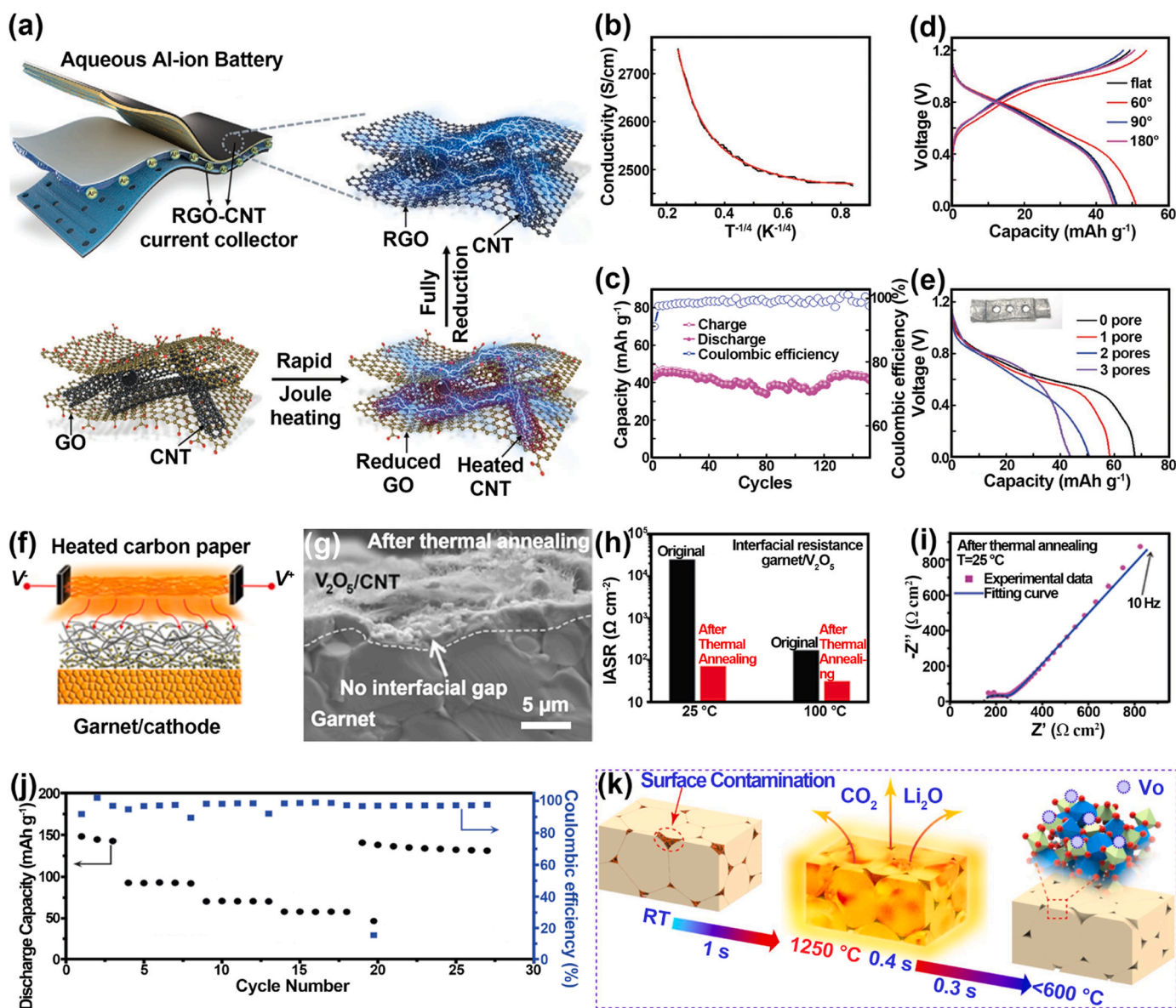

Fig. 11. (a) The preparation of GO-CNT triggered by Joule heating process. (b) The conductivity of the rGO-CNT film reduced by CTS process. (c) The cycle stability test of the AIBs. (d) The discharge capacity of the aqueous AIB. (e) The charge/discharge tests of the aqueous AIBs punched by several holes. Reproduced with permission [30]. Copyright 2018, Wiley-VCH. (f) The diagram of rapid thermal annealing device. (g) the cross-section SEM image of the garnet SSE and cathode after thermal annealing. (h) The interfacial charge transfer resistance with comparison of before and after rapid thermal annealing. (i) EIS of cathode symmetric cell. (j) Discharge capacity and Coulombic efficiency of the Li/garnet/V_2O_5 full cell. Reproduced with permission [117]. Copyright 2017, American Chemical Society. (k) The diagram of rapid pulse thermal treatment process of garnet SSE. Reproduced with permission [120]. Copyright 2018, Elsevier.

sheet resistance ($0.8 \, \Omega \, \text{sq}^{-1}$) by high-temperature Joule heating method. The good electrical conductivity of graphene oxide films has been proven by molecular dynamics simulations (MDS) to be due to interlayer bridging bonds that flaws encourage and are brought about by the improved reactivity of carbon atoms at the edges of defects at high temperatures. The electrochemical performance of Li-ion batteries when highly conductive rGO sheets were used as the current collector was superior to that of a standard Al current collector.

To resolve the outstanding problems of feeblish electrical conductivity and weaker mechanical strength of CNT-based fibers, Wang et al. [70] modified CNT fibers with 1,3,5-tris (2′-bromophenyl) benzene (2TBB) molecules via a nanosoldering technique triggered through the CTS process, which formed covalent bond bridging between CNTs and 2TBB molecules. This resulted in a nearly 100-times increase in electrical conductivity and a 47% increase in tensile strength. Liu and co-workers [30] reported an rGO-CNT hybrid film via high-temperature reducing of GO-CNT hybrid film, which was employed as free-standing flexible current collector of aqueous AIBs (Fig. 11a). The Joule heating process started on CNTs (shown by the red tubes), and as the electrifying time grows, the functional groups on GO progressively shrink. As current collectors, fully reduced rGO-CNT is constructed in flexible water-based AIBs with good mechanical and electrical conductivity. The rGO-CNT hybrid film exhibited high electrical conductivity ($2750 \, \text{S} \, \text{cm}^{-1}$) (Fig. 11b), excellent flexibility and scalability. The CuHCF cathode, MoO_3 anode, and rGO-CNT sheets current collector in the as-assembled aqueous Al-ion complete cell demonstrated outstanding electrochemical performance with commendable cycle performance (Fig. 11c). Furthermore, the AIBs show excellent flexibility and patience to mechanical damages, such as punching, folding, bending, and cutting without adverse damages to the electrochemical performance (Fig. 11d-e).

Due to their high-temperature thermal and electrochemical stability, ceramic-based solid-state electrolytes (SSEs), an essential component of high-temperature all-solid-state batteries, have recently been able to resolve the vexing safety problems associated with conventional liquid organic electrolytes for high-temperature batteries [114]. For garnet SSE, the impracticable interface issue between the SSE and the cathode is still not well-addressed due to the long high-temperature processing or sintering processes [115,116]. In this regard, Liu et al. [117] employed a rapid Joule heating treatment technique to anneal the interface between $Li_7La_{2.75}Ca_{0.25}Zr_{1.75}Nb_{0.25}O_{12}$ (LLCZNO) garnet SSE and V_2O_5 cathode, forming a firm and continuous interface due to the fusion of the melt V_2O_5 cathode and LLCZNO garnet SSE at high temperature (Fig. 11f-g). The resulting cathode/garnet interfacial impendence was remarkably reduced from $2.5 \times 10^4 \, \Omega \, \text{cm}^2$ to $71 \, \Omega \, \text{cm}^2$ at room temperature and from $170 \, \Omega \, \text{cm}^2$ to $31 \, \Omega \, \text{cm}^2$ at $100 \, °\text{C}$ (Fig. 11h), respectively. Moreover, the diffusion impendence inside the V_2O_5 cathode was also substantially reduced (Fig. 11i). Based on the totally solid-state battery components, the high-temperature Li metal battery with small interfacial resistance ($45 \, \Omega \, \text{cm}^2$) delivered excellent electrochemical performance at $100 \, °\text{C}$ (Fig. 11j). Due to the high reactivity and mobility of Li ions, SSEs were Li conductive ceramic materials that were vulnerable to surface contamination and ceramic degradation. This resulted in inadequate interfacial transport of Li ions, which negatively impacted the electrochemical performance [118]. Peculiarly, lithium carbonate (Li_2CO_3) contamination preferentially accumulates on the surface/grain boundaries of aged garnet SSEs, hampering the practical commercialization process of solid-state batteries [119]. To address this issue, Wang et al. [120] proposed a thermal shock method for $< 2 \, \text{s}$ at $1250 \, °\text{C}$ to cleanse Li_2CO_3 contamination from the surface and grain boundaries of $Li_7La_3Zr_2O_{12}$ (LLZO) ceramic-based garnet SSEs (Fig. 11k). The ultrafast processing time couldalso concurrently introduce oxygen vacancies in the SSEs, besides impeding Li evaporation loss and phase change of the SSEs. The formation mechanism of oxygen vacancies was systematically investigated, leading toa 2-fold increase of ionic conductivity ($3.2 \times 10^{-4} \, \text{S} \, \text{cm}^{-1}$) compared to untreated EESs solid-state electrolyte ($1.6 \times$

$10^{-4} \, \text{S} \, \text{cm}^{-1}$). Capitalizing on these attributes, the thermal-shocktreated garnet SSE exhibited enhanced electrochemical cycling stability. In consequence, the symmetric Li/SSE/Li cells equipped with thermal-shock treated garnet SSE could cycle at $500 \, \mu\text{A} \, \text{cm}^{-2}$current density, whereas the untreated counterparts suffered froma short circuit at $100 \, \mu\text{A} \, \text{cm}^{-2}$.

4.2.2. Li-ion battery

Li-ion batteries (LIBs), as the mainstream EES device, have dominated the energystorage market due to their remarkable energy densities. However, there are still huge challenges in developing novel materials or modifying the components to satisfy the ever-increasing requirements for LIBs. The advent of CTS technique has ushered in a new era for the advancement of Li-based energy storage devices.

Active electrode materials loaded on highly conductive carbon supports can facilitate electron transport in the charge-discharge process. Chen and co-workers [59] designed ultrafine Si, Sn and Al NPs anchored on the rGO substrate via high temperature CTS procedure (Fig. 12a). When served as the anode of LIBs, the rGO-Si NPs film delivered a high discharge specific capacitance ($3367 \, \text{mA h} \, \text{g}^{-1}$), a superior volumetric capacity ($3543 \, \text{mA h} \, \text{cm}^{-3}$), an outstanding areal capacity ($2.48 \, \text{mA h} \, \text{cm}^{-2}$) at $0.13 \, \text{mA} \, \text{cm}^{-2}$, together with excellent cycling stability (Fig. 12b-c), surpassing those of the rGO-Si MPs film electrodes. The inferior stability of the solid electrolyte interface induced by high activation surface area of NP-based battery electrodes had pushed microparticles (submicron to micron) to the foreground in battery fields [121,122]. Recently, Dong and co-workers [85] reported HEO microparticles and applied them as LIB anode material (Fig. 12d). To fill a homogenous mixture of metal salt precursors and achieve good heat transmission efficiency, flexible carbon heat processors were formed into the necessary shape. The $(Mn, Fe, Co, Ni, Cu, Zn)_3O_{4-x}$ HEO microparticles electrode demonstrated outstanding cycling performance with 90% capacitance retention after 100 cycles at C/5 and a superior Coulombic efficiency of nearly 98%, in addition to outstanding rate performance, in a typical half-cell configuration. (Fig. 12e-f). Dendrite growth and interface instability of Li metal anodes were the notorious issues of Li metal-based batteries, which could effectively be solved by employing a heterogeneous seed induction strategy. In this regard, Yang and co-workers [60] prepared homogeneous Ag NPs ($\sim 40 \, \text{nm}$) on CNFs via CTS method, which could effectively tune the deposition behavior of Li, guided uniform Li deposition in a 3D carbon framework, and suppress the formation of Li dendrites. In a consequence, the modified Li metal anode with Ag nanoseeds exhibited an unrivaled cycling stability for $500 \, \text{h}$ at $0.5 \, \text{mA} \, \text{cm}^{-2}$ without short-circuiting, which was remarkably superior to the bare CNF substrates ($< 100 \, \text{h}$) (Fig. 12g-h). Lu and co-workers [123] proposed an efficient and high-value recycling method that converts high-purity WSi to stable 1D Si nanowires (SiNWs) on the GO substrate via a high temperature electrothermal shock technique (Fig. 12i). The Si atoms in the WSi powder, produced at high temperature ($2100 \, \text{K}$), directionally diffuse to form SiNWs between GO films, thereby forming a conductive and self-supporting SiNWs@rGO composite (Fig. 12j). When used as the anode of LIBs, the SiNWs@rGO electrode with 76% Si content delivered superior initial Coulombic efficiency (ICE) of 89.5% (Fig. 12k), and excellent cycling performance with $2381.7 \, \text{mAh} \, \text{g}^{-1}$ for more 500 cycles at $1 \, \text{A} \, \text{g}^{-1}$ (Fig. 12l). Furthermore, full LIBs paired with commercial $Li[Ni_{0.8}Co_{0.16}Al_{0.04}]O_2$(NCA) cathode displayed outstanding cycling stability with $126.3 \, \text{mAh} \, \text{g}^{-1}$ at $0.2 \, \text{C}$ for 100 cycles, as well as superior energy density of $454.7 \, \text{W h} \, \text{kg}^{-1}$. Recently, in view of the complicated multistep reaction process and sluggish reaction dynamics issues existing in conventional synthesis methods of cathode materials for LIBs, Zhu et al. [124] synthesized a series of typical cathode materials for LIBs with high purity, abundant oxygen vacancy, ultrafine particle size and excellent electrochemical performance, such as $LiFePO_4$, $LiCoO_2$, $LiMn_2O_4$ and xLiMO$_2$·$(1 - x)$Li$_2$MnO$_3$ (M=Ni, Co, Mn)/NiO composite material, via high-temperature carbothermal shock technique using acetate-based
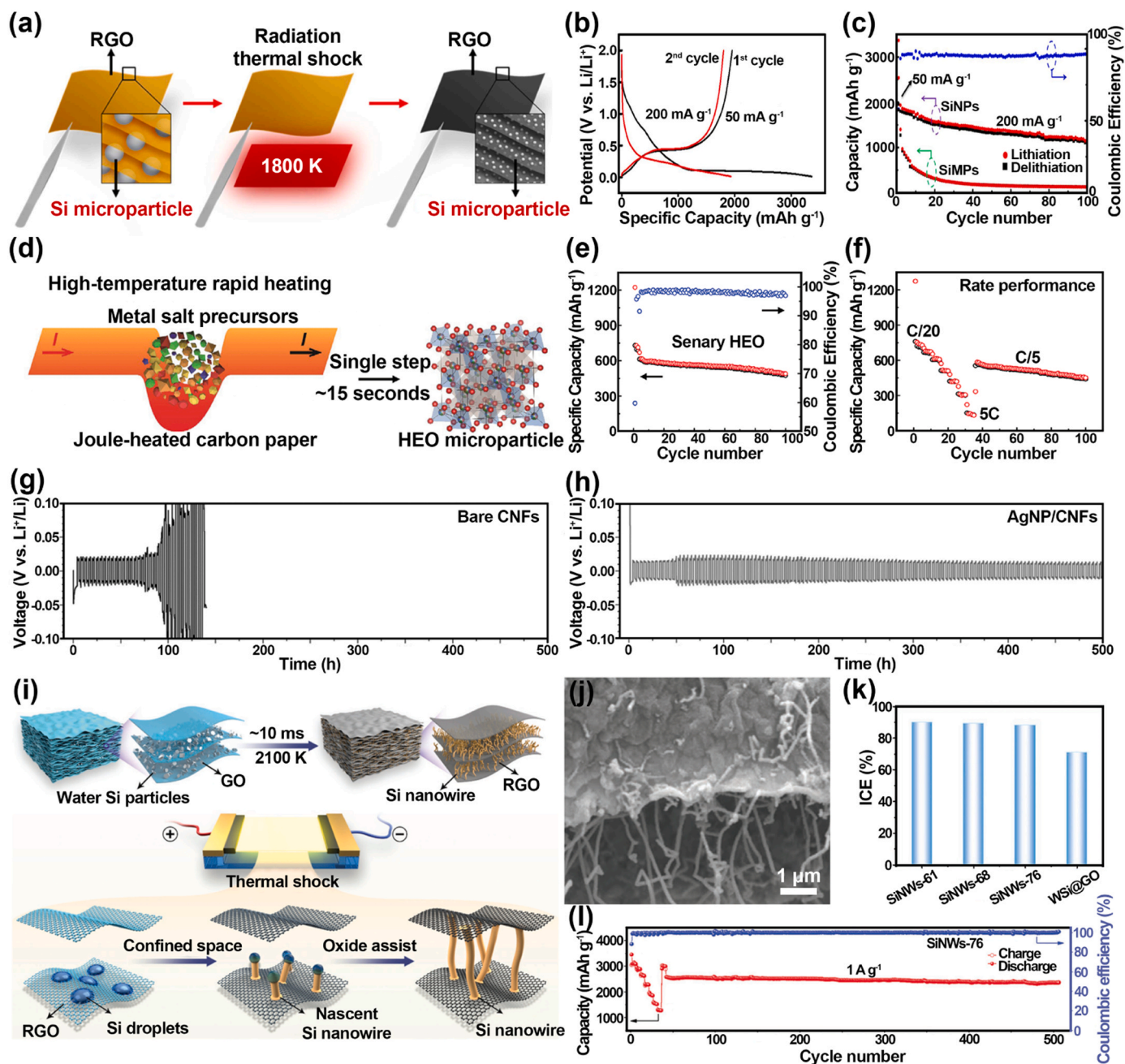
Fig. 12. (a) Rapid preparation of rGO-SiNPs on hot rGO paper. (b) Galvanostatic discharge/charge profiles of the rGO-SiNPs film of the first two times cycle. (c) Cycling test of the rGO-SiNPs and rGO-SiMPs films. Reproduced with permission [59]. Copyright 2016, American Chemical Society. (d) The high-temperature Joule heating process featured a fast thermal treatment for just seconds. (e) Cycling performance of the senary HEO using a half-cell configuration at C/5. (f) The rate performance of the senary HEO. Reproduced with permission [85]. Copyright 2022, Wiley-VCH. Cycling performance of Li anode plating/stripping on (g) bare CNFs and (h) AgNP/CNFs. Reproduced with permission [60]. Copyright 2017, Wiley-VCH. (i) The schematic of the CTS process for synthesizing SiNWs. (j) Cross section SEM images of the film. (k) Starting Coulombic efficiency comparison. (l) Rate capacity of the SiNWs-76 electrode. Reproduced with permission [123]. Copyright 2021, Wiley-VCH.

precursor obtained by combustion method.

4.2.3. Li-air battery

Rechargeable Li-O$_2$ batteries, which featureultra-high energy density ($\sim$ 3500 Wh kg^{-1}), have been extensively investigated to satisfy the ever-increasing requirement for high-energy devices, involving ORR during the discharge process on the cathode and OER during the charge process [125]. Thus, designing and exploiting advanced catalysts for ORR and OER is vital to enhance the electrochemical performance of Li-O$_2$ batteries. Jung and co-workers [126] synthesized quaternary

polyelemental (Au, Pd, Pt, and Ru) NPs loaded on CNFs through the high-temperature CTS method (Fig. 13a). The PtPdAuRu/CNF NPs electrode delivered a reduced overpotential (0.45 V) and a high discharge capacitance (9130 mAh g^{-1}), which was about three times more than that of the pristine CNF (Fig. 13b-c). The excellent electrochemical performance was ascribed to the enhanced catalytic activity related to the appropriate O$_2$ adsorption ability of the PtPdAuRuNPs.

Due to its cheap cost-effectiveness, safety, and high theoretical energy density, zinc-air batteries (ZABs), which are promising energy storage devices, have attracted a lot of attention [127,128]. The
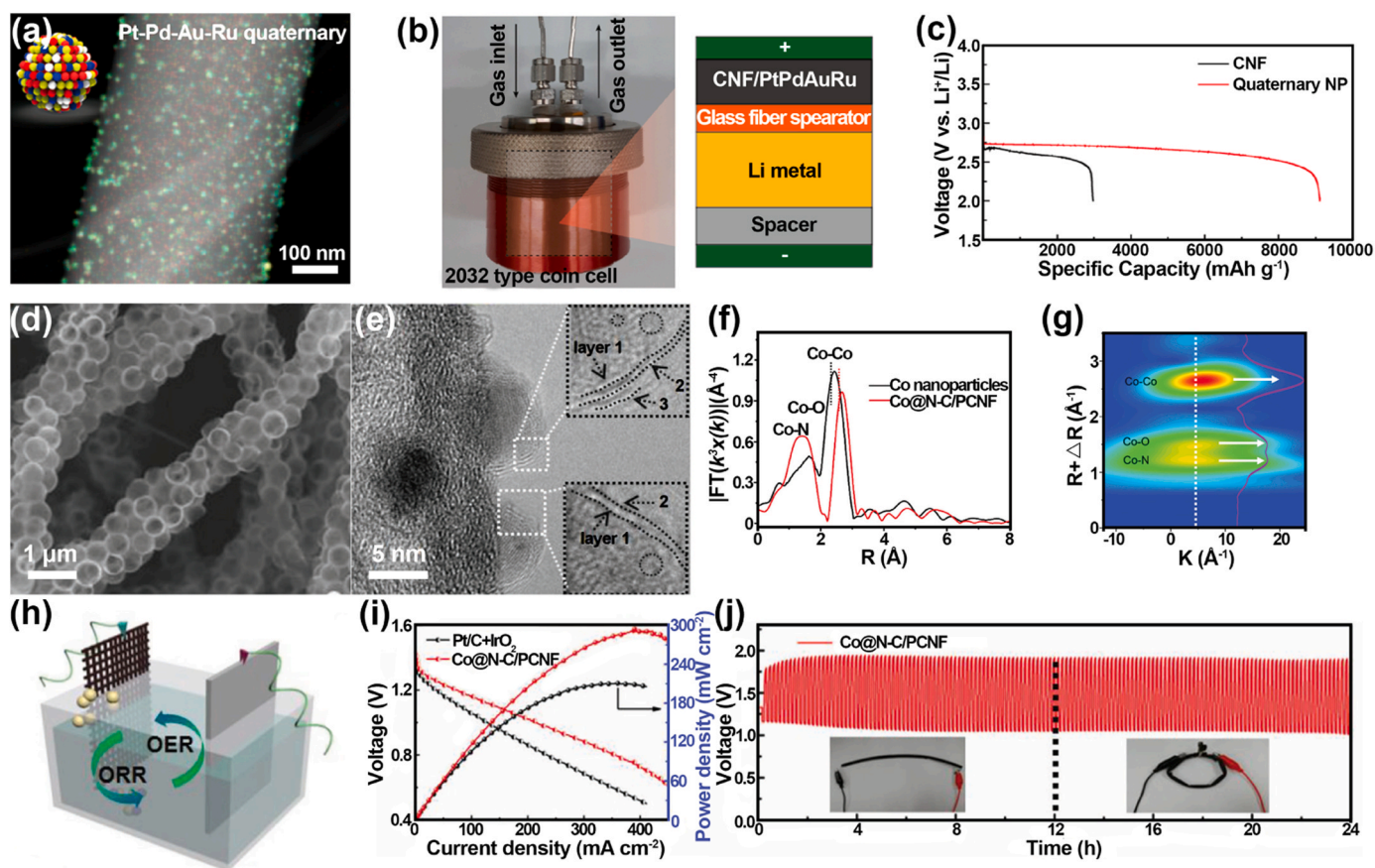
Fig. 13. (a) Element mapping of Pt-Pd-Au-Ru nanoparticles. (b) Diagram of Li-O$_2$ single-cell equipment and its composition. (c) Discharge curves of the CNF and CNF/Pt-Pd-Au-Ru electrodes. Reproduced with permission [126]. Copyright 2021, American Chemical Society. (d) SEM images of the Co@N-C/PCNF composite. (e) HRTEM image of Co@N-C nanoparticle. (f) R-space spectra depicting the Co K-edge in both Co nanoparticles and Co@N-C/PCNF. (g) WT-EXAFS of the Co K-edge in Co@N-C/PCNF. (h) Diagram of aqueous ZABs. (i) Corresponding discharge polarizations and power density curves. (j) Stability test of Co@N-C/PCNF-based flexible ZAB. Reproduced with permission [131]. Copyright 2021, Wiley-VCH.

electrochemical performance of ZABs intensely rests with the efficiency of ORR/OER [129]. The adsorption/desorption kinetics of intermediates accelerated by TM-N-C moieties in the OER/ORR procedure were proposed [130]. Unfortunately, several factors still need to be optimized for the TM@N-C-based catalysts, such as limited active sites exposure, inferior electronic conductivity, untight contact of TMs and carbon substrate, and aggregation of TMs. Therefore, it is pivotal to explore efficient methods to synthesize low-cost, stable, and efficient TM@N-C catalysts. In this regard, Lu and co-workers [131] prepared core-shell structure Co@N-C/PCNF catalysts via CTS shock technology. The as-fabricated Co@N-C/PCNF featured with inimitable advantages, such as high graphitization degree, highly dispersed and homogeneous distribution of Co NPs, ultrathin N-doped carbon shell, and large SSA (Fig. 13d-e), which was favorable for the pace of mass transfer and exposure of active sites. Benefiting from these merits, the Co@N-C/PCNF composites exhibited remarkable reversible oxygen electrocatalytic activityat both OER and ORR. Moreover, the experimental and simulation results jointly validated that the electrical structure and local environmental of Co in the composite can be tuned at the interface of Co-N-C moiety (Fig. 13f-g), thus optimizing the adsorption/desorption energy of oxygen intermediated and speeding up the reaction kinetic of OER/ORR, further improving the electrocatalytic activities. Simultaneously, when used as air electrodes, the Co@N-C/PCNF composite-based aqueous ZABs exhibited a high specific capacitance of 292 mW cm^{-2} (Fig. 13h-i), while the flexible ZABs also delivered excellent electrochemical activity with high specific capacity and long cycling lifespan (Fig. 13j). In another work, the as-obtained well-structure NiCo LDH@CC was chosen as the cathode material of

zinc-ion batteries (ZIBs), delivering admirable energy density of 301.7 Wh kg^{-1}, superior cycling stability of 81.4% capacitance retention after 5000 cycles at 15 A g^{-1}. In addition, the as-assembled flexible quasi-solid-state zinc-ion micro-batteries (ZIMBs) using PVA-KOH as an electrolyte also presented remarkable specific capacitance, superior energy density, together with prominent long-term stability [132]. Recently, Li and co-workers [133] successfully synthesized various element (Fe, Mn, Ni, Zn, and Mg) doped CoO electrocatalysts via a feasible and fast Joule heating technique. The resultant Fe-CoO materials exhibited splendid OER activity with an overpotential as low as 280 mV at 10 mA cm^{-2} and remarkable cycling stability. The ZABs assembled with Fe-CoO and Mn-CoO delivered high power density (305 mW cm^{-2}), superior durability, together with remarkable long-term stability (> 450 cycles at 5 mA cm^{-2}).

Due to its high theoretical energy density, Li-CO$_2$ batteries have been recognized as promising energy storage technologies that could lessen the "greenhouse effect" by absorbing CO$_2$ and fully utilizing the surplus CO$_2$ in the atmosphere [134,135]. Unfortunately, Li-CO$_2$ batteries are subjected to several bottlenecks, such as poor rechargeability, low recyclability, inferior rate performance, and low Coulombic efficiency [136]. To enhance the electrochemical performance of Li-CO$_2$ batteries, it is therefore potential to develop and build highly efficient cathodes. The energy storage and power density of Li-CO$_2$ batteries are thought to be improved by designing thick electrodes, which increase the area mass load of active materials and decrease the weight to volume ratio of inactive material [137]. In this regard, Ni NPs@rGO produced using the CTS process (1900 K for 54 ms) was used by Qiao and colleagues to construct an ultrathick cathode (0.4 mm) for a high energy density

Li-CO$_2$ battery. The Ni/rGO cathode provided a low overpotential of 1.05 V at 100 mA g^{-1}, a high areal capacitance (14.6 mA h cm^{-2}), outstanding cycling stability (100 cycles), and superior rate capability (up to 1000 mA g^{-1}). This was made possible by the thick electrode and uniform dispersion of Ni NPs. On activated CNFs (ACNFs), the same team created highly dispersion and ultrafine Ru NPs that were used as a high-efficiency cathode for Li-CO$_2$ batteries [138]. The Ru/ACNFs electrode demonstrated a low overpotential voltage (1.43 V) over 50 cycles at 0.1 A g^{-1} and enhanced cycling stability thanks to the ultrafine Ru NPs (4.1 ± 0.9 nm), multi-channel routes (given by cross-linked nanofibers), and porous structure (supplied by ACNFs). In addition, even at high current densities (0.8 and 1.0 A g^{-1}), low overpotentials (1.79 and 1.81 V, respectively) could be achieved, displaying remarkable rate performance and admirable reversibility.

In summary, CTS technology has shown a wide range of application potential in the field of rechargeable batteries. The ultra-high processing temperature and extremely fast rising and cooling rate based on CTS give the material well mechanical properties, which also has significant advantages in slowing dendrite growth and increasing battery durability. The modification treatment of separator is a blank of CTS technology in energy storage fields, and needs further exploration.

5. Conclusions and future outlook

In this review, the CTS technique featured extremely fast heating/cooling rates is systematically introduced. Firstly, the development history, equipment and advantages of the CTS technique are briefly introduced. Subsequently, versatile nanomaterials obtained via the CTS technique are presented, including metal NPs, carbon-based nanomaterials, and compound nanomaterials (e.g., carbides, oxides, phosphides, transition metal sulfides/borides, and high-entropy compounds). Finally, the versatile applications of these nanomaterials are exhaustively elaborated, including energy-related electrocatalytic fields (e.g., HER, OER, ORR, CO$_2$RR, NRR), rechargeable batteries. In recent years, although plenty of research works based on the CTS technique have been deliberately investigated, there are still considerable spaces for development. Hence, in our opinion, future perspectives and valuable research directions will focus on the following aspects (Fig. 14):

(1) The CTS setup linked with aerosol spray pyrolysis method or roll-to-roll possessing technique enables the large-scale preparation of nanomaterials. Moreover, apart from the routine utilized substrate (CNF, CNT, GO) as heater, there are several advanced heaters for CTS setup, such as graphite paper, face-to-face carbon paper. Therefore, coupled with other preparation technique of nanomaterials, seeking and designing new-style heater with unique structure (e.g., bowland boat) to obtain functional materials are the uppermost search directions for the modification of CTS setup in the near future. What's more, defects or junctions in carbon substrates would become high-temperature zones in the process of Joule heating. Therefore, whether the carbon substrate can render efficient heat conduction or dissipation from high-temperature spots to obtain homogeneous temperature field is essential for better control of product uniformity.

(2) Nanomaterials prepared via the CTS technique universally exhibit the nanoscale sphere-like particles, unavailable sophisticated and diverse hierarchical and heterostructures (e.g., core-shell, hollow, multi-shell), selected crystal planes, as well as the surface functionalization, which further hamper their comprehensive application in various fields. In addition, the current research primarily on the preparation of transition metal sulfides and high-entropy alloys in terms of compound nanomaterials. The CTS technique should be extended to a series of other compound nanomaterials (e.g., phosphides, oxides, nitrides), which have garnered recognition in the energy storage and conversion fields. Therefore, reasonable designing the CTS process (e.g., cooling medium, heating period, and secondary treatment) and choosing rational precursors to obtain novel compound functional materials also shows high significance. Additionally, obtaining the kilograms-quantity nanomaterials with CTS technique remains a challenge. Last but not least, the formation mechanism of these nanomaterials remains mostly vague owing to the ultrafast synthesis process. It is anticipated that an intimate integration with in silico simulations and operando characterizations will yield important insights and empower future research of ultrafast synthesis.

(3) For carbon-based materials, the current research mainly focused on two aspects: one is the treatment of carbon-based nanomaterials (e. g. welding CNFs, healing the defect of graphene fibers, and high-temperature annealing), and the other is the preparation of porous carbon nanomaterials (high-temperature carbonized biomass). The former has been extensively studied. Unfortunately, the mechanistic details of how these carbon-based nanomaterials are converted have remained intangible. In comparison, the preparation of carbon-based nanomaterials via CTS technique has been less investigated. Thus, selecting other biomass or coal-chemical byproducts as precursors, combined
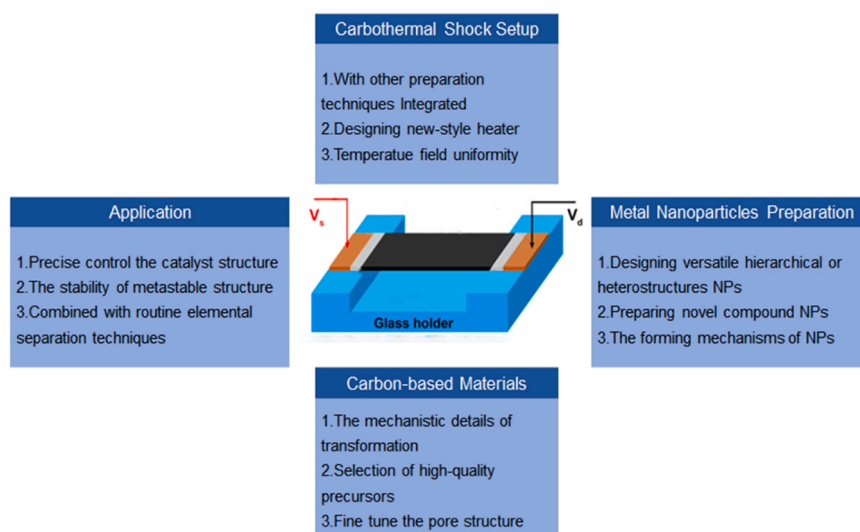

Fig. 14. Illustration of the future research direction toward carbothermal shock techniques.

with template-activation strategy to tune the pore structure and size will be an important research direction for the preparation of the hierarchical pore carbon via the CTS method. How to better tune carbon structures by fine adjusting the synthesis parameters in the process of carbonization is critical.

(4) The CTS technique can promote the progress of batteries and catalysts. It shows promising potentials in electrochemical energy storage devices (Li-based batteries, Zn-air batteries, Na-ions batteries, and supercapacitors) and energy conversion devices (HER, OER, ORR, and NRR). For energy storage devices, the research hotspot mainly focuses on the preparation of anode, cathode, current collector, and the modification treatment of solid electrolyte. The modification treatment of separator is a blank of CTS technology in energy storage fields, and needs further exploration. Moreover, for energy conversion fields, novel catalysts for CO_2RR and CO oxidation/reduction are urgently needed to achieve the "carbon neutral" goal. In addition, how to precise control the catalyst structure and whether the metastable structure remains stable during the electrocatalytic process are all outstanding and challenging questions.

(5) The utilization of CTS technique can facilitate the advancement of waste recycling in order to fulfill the demands of a circular economy.To date, the high-purity silicon waste, coal fly ash, bauxite slag, and e-waste as the goal waste have been investigated to obtain high-added value materials via the CTS technique. Therefore, exploring the treatment of other waste (e.g., metallurgical slag) and purifying of sea water to obtain valuable elements can be valuable research directions for the CTS technique. Meanwhile, combining the commercial elemental separation techniques (e.g., ion exchange and solvent extraction) with CTS technique will be an effective and feasible route to realize scalable application.

In short, the emerging CTS technique holds significant significance in producing adaptable functional nanomaterials and exhibits immense potential in diverse domains, particularly in the realm of electrochemical energy storage and conversion. We anticipate that above-mentioned issues can be better resolved in the future research and render the CTS technique to be the mainstream material preparation methods. Predictably, the bright prospects of CTS technology in energy storage and conversion will accelerate the development of the next generation of energy-related devices.

CRediT authorship contribution statement

Wei Zhang: Conceptualization, Investigation, Writing. **Xiang Wei:** Conceptualization, Investigation, Writing. **Tong Wu:** Conceptualization, Investigation, Writing. **Feng Wei:** Investigation. **Lianbo Ma:** Investigation. **Yaohui Lv:** Writing – review & editing, Supervision. **Weijia Zhou:** Writing – review & editing, Supervision. **Hong Liu:** Writing – review & editing, Supervision.

Declaration of Competing Interest

The authors declare that they have no known competing financial interests or personal relationships that could have appeared to influence the work reported in this paper.

Data Availability

No data was used for the research described in the article.

Acknowledgements

Appendix A. Supporting information

Supplementary data associated with this article can be found in the online version at doi:10.1016/j.nanoen.2023.108994.

References

[1] S. Mu, Q. Liu, P. Kidkhunthod, X. Zhou, W. Wang, Y.B. Tang, Molecular grafting towards high-fraction active nanodots implanted in N-doped carbon for sodium dual-ion batteries, Natl. Sci. Rev. 8 (2021) nwaa178.

[2] J.M. Luo, H.N. Han, X.L. Wang, X.Z. Qiu, B. Liu, Y.L. Lai, X.Y. Chen, R.M. Zhong, L. Wang, C.Y. Wang, Single-atom Nb anchored on graphitic carbon nitride for boosting electron transfer towards improved photocatalytic performance, Appl. Catal. B-Environ. 328 (2023), 122495.

[3] Y. Pei, G. Zhou, N. Luan, B. Zong, M. Qiao, F.F. Tao, Synthesis and catalysis of chemically reduced metal-metalloid amorphous alloys, Chem. Soc. Rev. 41 (2012) 8140–8162.

[4] D.X. Luong, K.V. Bets, W.A. Algozeeb, M.G. Stanford, C. Kittrell, W. Chen, R. V. Salvatierra, M. Ren, E.A. McHugh, P.A. Advincula, Z. Wang, M. Bhatt, H. Guo, V. Mancevski, R. Shahsavari, B.I. Yakobson, J.M. Tour, Gram-scale bottom-up flash graphene synthesis, Nature 577 (2020) 647–651.

[5] L. Li, J. Zhang, Y. Wang, F.U. Zaman, Y. Zhang, L. Hou, C. Yuan, Laser irradiation construction of nanomaterials toward electrochemical energy storage and conversion: ongoing progresses and challenges, InfoMat 3 (2021) 1393–1421.

[6] Y. Shi, Y. Wang, J. Yu, Y. Chen, C. Fang, D. Jiang, Q. Zhang, L. Gu, X. Yu, X. Li, H. Liu, W. Zhou, Superscalar phase boundaries derived multiple active sites in $SnO_2/Cu_6Sn_5/CuO$ for tandem electroreduction of CO_2 to formic acid, Adv. Energy Mater. 13 (2023), 2203506.

[7] X. Liu, C. Xing, F. Yang, Z. Liu, Y. Wang, T. Dong, L. Zhao, H. Liu, W. Zhou, Strong interaction over Ru/defects-rich aluminium oxide boosts photothermal CO_2 methanation via microchannel flow-type system, Adv. Energy Mater. 12 (2022), 2201009.

[8] G. Xiong, Y. Chen, Z. Zhou, F. Liu, X. Liu, L. Yang, Q. Liu, Y. Sang, H. Liu, X. Zhang, J. Jia, W. Zhou, Rapid synthesis of various electrocatalysts on Ni foam using a universal and facile induction heating method for efficient water splitting, Adv. Funct. Mater. 31 (2021), 2009580.

[9] G. Xiong, J. Jia, L. Zhao, X. Liu, X. Zhang, H. Liu, W. Zhou, Non-thermal radiation heating synthesis of nanomaterials, Sci. Bull. 66 (2021) 386–406.

[10] X. Shi, M. Fields, J. Park, J.M. McEnaney, H. Yan, Y. Zhang, C. Tsai, T. F. Jaramillo, R. Sinclair, J.K. Nørskov, X. Zheng, Rapid flame doping of Co to WS_2 for efficient hydrogen evolution, Energy Environ. Sci. 11 (2018) 2270–2277.

[11] Y. Tian, L. Yu, C. Zhuang, G. Zhang, S. Sun, Fast synthesis of Pt single-atom catalyst with high intrinsic activity for hydrogen evolution reaction by plasma sputtering, Mater. Today Energy 22 (2021), 100877.

[12] Y. Yao, Z. Huang, P. Xie, S.D. Lacey, R.J. Jacob, H. Xie, F. Chen, A. Nie, T. Pu, M. Rehwoldt, D. Yu, M.R. Zachariah, C. Wang, R. Shahbazian-Yassar, J. Li, L. Hu, Carbothermal shock synthesis of high-entropy-alloy nanoparticles, Science 359 (2018) 1489–1494.

[13] Y. Liu, Z. Ge, Z. Li, Y. Chen, High-power instant-synthesis technology of carbon nanomaterials and nanocomposites, Nano Energy 80 (2021) 105500.

[14] L. Lai, J. Li, Y. Deng, Z. Yu, L. Wei, Y. Chen, Carbon and carbon/metal hybrid structures enabled by ultrafast heating methods, Small Struct. 3 (2022), 2200112.

[15] Q. Liu, S. Chen, Ultrafast synthesis of electrocatalysts, Trends Chem. 4 (2022) 918–934.

[16] X. Hu, D. Zuo, S. Cheng, S. Chen, Y. Liu, W. Bao, S. Deng, S.J. Harris, J. Wan, Ultrafast materials synthesis and manufacturing techniques for emerging energy and environmental applications, Chem. Soc. Rev. 52 (2023) 1103–1128.

[17] Q. Liu, B. Lu, F. Nichols, J. Ko, R. Mercado, F. Bridges, S. Chen, Rapid preparation of carbon-supported ruthenium nanoparticles by magnetic induction heating for efficient hydrogen evolution reaction in both acidic and alkaline media, SusMat 2 (2022) 335–346.

[18] C. Huang, Y. Wang, R. Zhong, Z. Sun, Y. Deng, L. Duan, Induction heating enables efficient heterogeneous catalytic reactions over superparamagnetic nanocatalysts, Chin. Chem. Lett. (2022), 108101.

[19] C. Meng, M. Lin, X. Sun, X. Chen, X. Chen, X. Du, Y. Zhou, Laser synthesis of oxygen vacancy-modified CoOOH for highly efficient oxygen evolution, Chem. Commun. 55 (2019) 2904–2907.

[20] Z. Li, Jian-Y. Fu, Y. Feng, C. Dong, H. Liu, X. Du, A silver catalyst activated by stacking faults for the hydrogen evolution reaction, Nat. Catal. 2 (2019) 1107–1114.

[21] F. Chen, Y. Yao, A. Nie, S. Xu, J. Dai, E. Hitz, Y. Li, A. Lu, Z. Huang, T. Li, R. Shahbazian-Yassar, L. Hu, High-temperature atomic mixing toward well-dispersed bimetallic electrocatalysts, Adv. Energy Mater. 8 (2018), 1800466.

[22] Y. Yao, F. Chen, A. Nie, S.D. Lacey, R.J. Jacob, S. Xu, Z. Huang, K. Fu, J. Dai, L. Salamanca-Riba, M.R. Zachariah, R. Shahbazian-Yassar, L. Hu, In situ high temperature synthesis of single-component metallic nanoparticles, ACS Cent. Sci. 3 (2017) 294–301.

[23] Y. Li, T. Gao, Y. Yao, Z. Liu, Y. Kuang, C. Chen, J. Song, S. Xu, E.M. Hitz, B. Liu, R. J. Jacob, M.R. Zachariah, G. Wang, L. Hu, In situ "chainmail catalyst" assembly in

low-tortuosity, hierarchical carbon frameworks for efficient and stable hydrogen generation, Adv. Energy Mater. 8 (2018), 1801289.

[24] M. Cui, C. Yang, S. Hwang, B. Li, Q. Dong, M. Wu, H. Xie, X. Wang, G. Wang, L. Hu, Rapid atomic ordering transformation toward intermetallic nanoparticles, Nano Lett. 22 (2022) 255–262.

[25] Y. Yao, K.K. Fu, C. Yan, J. Dai, Y. Chen, Y. Wang, B. Zhang, E. Hitz, L. Hu, Three-dimensional printable high-temperature and high-rate heaters, ACS Nano 10 (2016) 5272–5279.

[26] Z. Liu, C. Duan, S. Dou, Q. Yuan, J. Xu, W.D. Liu, Y. Chen, Ultrafast porous carbon activation promises high-energy density supercapacitors, Small 18 (2022), 2200954.

[27] H. Wu, Q. Lu, J. Zhang, J. Wang, X. Han, N. Zhao, W. Hu, J. Li, Y. Chen, Y. Deng, Thermal shock-activated spontaneous growing of nanosheets for overall water splitting, Nano-Micro Lett. 12 (2020) 162.

[28] H. Qiao, X. Wang, Q. Dong, H. Zheng, G. Chen, M. Hong, C. Yang, M. Wu, K. He, L. Hu, A high-entropy phosphate catalyst for oxygen evolution reaction, Nano Energy 86 (2021), 106029.

[29] T. Li, Y. Yao, B.H. Ko, Z. Huang, Q. Dong, J. Gao, W. Chen, J. Li, S. Li, X. Wang, R. Shahbazian-Yassar, F. Jiao, L. Hu, Carbon-supported high-entropy oxide nanoparticles as stable electrocatalysts for oxygen reduction reactions, Adv. Funct. Mater. 31 (2021), 2010561.

[30] S. Liu, P. Wang, C. Liu, Y. Deng, S. Dou, Y. Liu, J. Xu, Y. Wang, W. Liu, W. Hu, Y. Huang, Y. Chen, Nanomanufacturing of RGO-CNT hybrid film for flexible aqueous Al-ion batteries, Small 16 (2020), 2002856.

[31] J.P. Joule, The scientific papers of James Prescott Joule, Cambridge University Press, 2011.

[32] M. Suda, Y. Takeda, K. Sujishi, T. Tanaka, Metabolism of tyrosine: III. Relation between homogentisicase, ferrous ion and L-ascorbic acid in experimental alcaptonuria of grinea pig, J. Biochem. 38 (1951) 297–302.

[33] P. Allia, M. Baricco, P. Tiberto, F. Vinai, Kinetics of the amorphous-to-nanocrystalline transformation in $Fe_{73.5}Cu_1Nb_3Si_{13.5}B_9$, J. Appl. Phys. 74 (1993) 3137–3143.

[34] R.S. Averback, H. Hahn, H.J. Höfler, J.C. Logas, Processing and properties of nanophase amorphous metallic alloys: Ni-Ti, Appl. Phys. Lett. 57 (1990) 1745–1747.

[35] F. El-Tantawy, Joule heating treatments of conductive butyl rubber/ceramic superconductor composites: a new way for improving the stability and reproducibility? Eur. Ploym. J. 37 (2001) 565–574.

[36] Z. Chen, X. Su, W. Wu, J. Zhou, T. Wu, Y. Wu, H. Xie, K. Li, Superhydrophobic PDMS@GSH wood with Joule heat and photothermal effect for viscous crude oil removal, Carbon 201 (2023) 577–586.

[37] K. Zhao, X. Li, D. Su, High-entropy alloy nanocatalysts for electrocatalysis, Acta Phys. Chim. Sin. 37 (2020), 2009077.

[38] H. Liu, L. Syama, L. Zhang, C. Lee, C. Liu, Z. Dai, Q. Yan, High-entropy alloys and compounds for electrocatalytic energy conversion applications, SusMat 1 (2021) 482–505.

[39] J.H. Los, K.V. Zakharchenko, M.I. Katsnelson, A. Fasolino, Melting temperature of graphene, Phys. Rev. B 91 (2015), 045415.

[40] D.D.Y. Touloukian, Thermal radiative properties: metallic elements and alloys, Plenum, New York, 1970.

[41] Y.D. Kim, H. Kim, Y. Cho, J.H. Ryoo, C.H. Park, P. Kim, Y.S. Kim, S. Lee, Y. Li, S. N. Park, Y.S. Yoo, D. Yoon, V.E. Dorgan, E. Pop, T.F. Heinz, J. Hone, S.H. Chun, H. Cheong, S.W. Lee, M.H. Bae, Y.D. Park, Bright visible light emission from graphene, Nat. Nanotechnol. 10 (2015) 676–681.

[42] S.B. Singer, M. Mecklenburg, E.R. White, B.C. Regan, Polarized light emission from individual incandescent carbon nanotubes, Phys. Rev. B 83 (2011), 233404.

[43] W. Bao, A.D. Pickel, Q. Zhang, Y. Chen, Y. Yao, J. Wan, K.K. Fu, Y. Wang, J. Dai, H. Zhu, D. Drew, M. Fuhrer, C. Dames, L. Hu, Flexible, high temperature, planar lighting with large scale printable nanocarbon paper, Adv. Mater. 28 (2016) 4684–4691.

[44] W. Chen, J.T. Li, Z. Wang, W.A. Algozeeb, D.X. Luong, C. Kittrell, E.A. McHugh, P. A. Advincula, K.M. Wyss, J.L. Beckham, M.G. Stanford, B. Jiang, J.M. Tour, Ultrafast and controllable phase evolution by flash Joule heating, ACS Nano 15 (2021) 11158–11167.

[45] Y. Qiu, Z. Hu, H. Li, Q. Ren, Y. Chen, S. Hu, Hybrid electrocatalyst Ag/Co/C via flash Joule heating for oxygen reduction reaction in alkaline media, Chem. Eng. J. 430 (2022), 132769.

[46] Y. Li, Y. Chen, A. Nie, A. Lu, R.J. Jacob, T. Gao, J. Song, J. Dai, J. Wan, G. Pastel, M.R. Zachariah, R.S. Yassar, L. Hu, In situ, fast, high-temperature synthesis of nickel nanoparticles in reduced graphene oxide matrix, Adv. Energy Mater. 7 (2017), 1601783.

[47] Y. Yao, Z. Huang, P. Xie, L. Wu, L. Ma, T. Li, Z. Pang, M. Jiao, Z. Liang, J. Gao, Y. He, D.J. Kline, M.R. Zachariah, C. Wang, J. Lu, T. Wu, T. Li, C. Wang, R. Shahbazian-Yassar, L. Hu, High temperature shockwave stabilized single atoms, Nat. Nanotechnol. 14 (2019) 851–857.

[48] Y. Liu, P. Li, F. Wang, W. Fang, Z. Xu, W. Gao, C. Gao, Rapid roll-to-roll production of graphene films using intensive Joule heating, Carbon 155 (2019) 462–468.

[49] X. Wang, Z. Huang, Y. Yao, H. Qiao, G. Zhong, Y. Pei, C. Zheng, D. Kline, Q. Xia, Z. Lin, J. Dai, M.R. Zachariah, B. Yang, R. Shahbazian-Yassar, L. Hu, Continuous 2000 K droplet-to-particle synthesis, Mater. Today 35 (2020) 106–114.

[50] Y. Qiao, C. Chen, Y. Liu, Y. Liu, Q. Dong, Y. Yao, X. Wang, Y. Shao, C. Wang, L. Hu, Continuous fly-through high-temperature synthesis of nanocatalysts, Nano Lett. 21 (2021) 4517–4523.

[51] Y. Yang, P. Ghildiyal, M.R. Zachariah, Thermal shock synthesis of metal nanoclusters within on-the-fly graphene particles, Langmuir 35 (2019) 3413–3420.

[52] Y. Chen, S. Xu, Y. Li, R.J. Jacob, Y. Kuang, B. Liu, Y. Wang, G. Pastel, L. G. Salamanca-Riba, M.R. Zachariah, L. Hu, FeS_2 nanoparticles embedded in reduced graphene oxide toward robust, high-performance electrocatalysts, Adv. Energy Mater. 7 (2017), 1700482.

[53] S. Liu, Z. Hu, Y. Wu, J. Zhang, Y. Zhang, B. Cui, C. Liu, S. Hu, N. Zhao, X. Han, A. Cao, Y. Chen, Y. Deng, W. Hu, Dislocation-strained IrNi alloy nanoparticles driven by thermal shock for the hydrogen evolution reaction, Adv. Mater. 32 (2020), 2006034.

[54] S. Zeng, B. Lv, J. Qiao, W. Yang, C. Zhu, Y. Zhang, D. Hu, M. Chen, J. Di, Q. Li, PtFe alloy nanoparticles confined on carbon nanotube networks as air cathodes for flexible and wearable energy devices, ACS Appl. Nano Mater. 2 (2019) 7870–7879.

[55] L. Zhang, J. Zhang, Q. Zheng, Y. Xu, X. Kou, T. Li, Formation of gold hollow spheres by rapid heating-cooling process, Gold. Bull. 55 (2022) 115–121.

[56] Y. Han, M. Liu, L. Sun, X. Li, Y. Yao, C. Zhang, S. Ding, H. Liao, L. Zhang, F. Fan, M. Moskovits, Z. Tian, A general strategy for overcoming the trade-off between ultrasmall size and high loading of MOF-derived metal nanoparticles by millisecond pyrolysis, Nano Energy 97 (2022), 107125.

[57] M. Cui, C. Yang, S. Hwang, M. Yang, S. Overa, Q. Dong, Y. Yao, A.H. Brozena, D. A. Cullen, M.F. Chi, T.F. Blum, D. Morris, Z. Finfrock, X. Wang, P. Zhang, V. G. Goncharov, X. Guo, J. Luo, Y. Mo, F. Jiao, L. Hu, Multi-principal elemental intermetallic nanoparticles synthesized via a disorder-to-order transition, Sci. Adv. 8 (2022) eabm4322.

[58] M. Jiao, Y. Yao, G. Pastel, T. Li, Z. Liang, H. Xie, W. Kong, B. Liu, J. Song, L. Hu, Fly-through synthesis of nanoparticles on textile and paper substrates, Nanoscale 11 (2019) 6174–6181.

[59] Y. Chen, Y. Li, Y. Wang, K. Fu, V.A. Danner, J. Dai, S.D. Lacey, Y. Yao, L. Hu, Rapid, in situ synthesis of high capacity battery anodes through high temperature radiation-based thermal shock, Nano Lett. 16 (2016) 5553–5558.

[60] C. Yang, Y. Yao, S. He, H. Xie, E. Hitz, L. Hu, Ultrafine silver nanoparticles for seeded lithium deposition toward stable lithium metal anode, Adv. Mater. 29 (2017), 1702714.

[61] Y. Yao, Z. Huang, P. Xie, T. Li, S.D. Lacey, M. Jiao, H. Xie, K.K. Fu, R.J. Jacob, D. J. Kline, Y. Yang, M.R. Zachariah, C. Wang, R. Shahbazian-Yassar, L. Hu, Ultrafast, controllable synthesis of sub-nano metallic clusters through defect engineering, ACS Appl. Mater. Interfaces 11 (2019) 29773–29779.

[62] J.Y. Song, C. Kim, M. Kim, K.M. Cho, I. Gereige, W.B. Jung, H. Jeong, H.T. Jung, Generation of high-density nanoparticles in the carbothermal shock method, Sci. Adv. 7 (2021) eabk2984.

[63] C. Liu, Y. Shen, J. Zhang, G. Li, X. Zheng, X. Han, L. Xu, S. Zhu, Y. Chen, Y. Deng, W. Hu, Multiple twin boundary-regulated metastable Pd for ethanol oxidation reaction, Adv. Energy Mater. 12 (2022), 2103505.

[64] C. Yang, B.H. Ko, S. Hwang, Z. Liu, Y. Yao, W. Luc, M. Cui, A.S. Malkani, T. Li, X. Wang, J. Dai, B. Xu, G. Wang, D. Su, F. Jiao, L. Hu, Overcoming immiscibility toward bimetallic catalyst library, Sci. Adv. 6 (2020) eaaz6844.

[65] P. Xie, Y. Yao, Z. Huang, Z. Liu, J. Zhang, T. Li, G. Wang, R. Shahbazian-Yassar, L. Hu, C. Wang, Highly efficient decomposition of ammonia using high-entropy alloy catalysts, Nat. Commun. 10 (2019) 4011.

[66] Y. Yao, Z. Huang, L.A. Hughes, J. Gao, T. Li, D. Morris, S.E. Zeltmann, B. H. Savitzky, C. Ophus, Y.Z. Finfrock, Q. Dong, M. Jiao, Y. Mao, M. Chi, P. Zhang, J. Li, A.M. Minor, R. Shahbazian-Yassar, L. Hu, Extreme mixing in nanoscale transition metal alloys, Matter 4 (2021) 2340–2353.

[67] Y. Yao, K.K. Fu, S. Zhu, J. Dai, Y. Wang, G. Pastel, Y. Chen, T. Li, C. Wang, T. Li, L. Hu, Carbon welding by ultrafast Joule heating, Nano Lett. 16 (2016) 7282–7289.

[68] S.H. Noh, W. Eom, W.J. Lee, H. Park, S.B. Ambade, S.O. Kim, T.H. Han, Joule heating-induced sp^2-restoration in graphene fibers, Carbon 142 (2019) 230–237.

[69] J.G. Kang, G. Wang, S.K. Kim, Joule heating-induced carbon fibers for flexible fiber supercapacitor electrodes, Materials 13 (2020) 5255.

[70] G. Wang, S.K. Kim, M.C. Wang, T. Zhai, S. Munukutla, G.S. Girolami, P. J. Sempsrott, S. Nam, P.V. Braun, J.W. Lyding, Enhanced electrical and mechanical properties of chemically cross-linked carbon-nanotube-based fibers and their application in high-performance supercapacitors, ACS Nano 14 (2020) 632–639.

[71] Y. Yao, F. Jiang, C. Yang, K.K. Fu, J. Hayden, C.F. Lin, H. Xie, M. Jiao, C. Yang, Y. Wang, S. He, F. Xu, E. Hitz, T. Gao, J. Dai, W. Luo, G. Rubloff, C. Wang, L. Hu, Epitaxial welding of carbon nanotube networks for aqueous battery current collectors, ACS Nano 12 (2018) 5266–5273.

[72] Y. Song, J. Di, C. Zhang, J. Zhao, Y. Zhang, D. Hu, M. Li, Z. Zhang, H. Wei, Q. Li, Millisecond tension-annealing for enhancing carbon nanotube fibers, Nanoscale 11 (2019) 13909–13916.

[73] Y. Chen, K. Fu, S. Zhu, W. Luo, Y. Wang, Y. Li, E. Hitz, Y. Yao, J. Dai, J. Wan, V. A. Danner, T. Li, L. Hu, Reduced graphene oxide films with ultrahigh conductivity as Li-ion battery current collectors, Nano Lett. 16 (2016) 3616–3623.

[74] J. Deng, M. Li, Y. Wang, Biomass-derived carbon: synthesis and applications in energy storage and conversion, Green. Chem. 18 (2016) 4824–4854.

[75] B.M. Matsagar, R. Yang, S. Dutta, Y.S. Ok, K.C.W. Wu, Recent progress in the development of biomass-derived nitrogen-doped porous carbon, J. Mater. Chem. A 9 (2021) 3703–3728.

[76] F. Zhang, Y. Yao, J. Wan, D. Henderson, X. Zhang, L. Hu, High temperature carbonized grass as a high performance sodium ion battery anode, ACS Appl. Mater. Interfaces 9 (2017) 391–397.

[77] F. Jiang, Y. Yao, B. Natarajan, C. Yang, T. Gao, H. Xie, Y. Wang, L. Xu, Y. Chen, J. Gilman, L. Cui, L. Hu, Ultrahigh-temperature conversion of biomass to highly conductive graphitic carbon, Carbon 144 (2019) 241–248.

[78] J. Pang, B. Chang, H. Liu, W. Zhou, Potential of MXene-based heterostructures for energy conversion and storage, ACS Energy Lett. 7 (2021) 78–96.

[79] H. Xie, K. Fu, C. Yang, Y. Yao, J. Rao, Y. Zhou, B. Liu, D. Kirsch, L. Hu, Necklace-like silicon carbide and carbon nanocomposites formed by steady Joule heating, Small Methods 2 (2018), 1700371.

[80] A. Cisquella-Serra, M. Magnani, M. Madou, M. Gamero-Castaño, Conformal CVD of WO_{3-x} on electrospun carbon nanofiber mats assisted by Joule heating, Carbon 195 (2022) 27–34.

[81] C. Yang, M. Cui, N. Li, Z. Liu, S. Hwang, H. Xie, X. Wang, Y. Kuang, D. Su, L. Hu, In situ iron coating on nanocatalysts for efficient and durable oxygen evolution reaction, Nano Energy 63 (2019), 103855.

[82] S. Xu, Y. Chen, Y. Li, A. Lu, Y. Yao, J. Dai, Y. Wang, B. Liu, S.D. Lacey, G.R. Pastel, Y. Kuang, V.A. Danner, F. Jiang, K.K. Fu, L. Hu, Universal, in situ transformation of bulky compounds into nanoscale catalysts by high-temperature pulse, Nano Lett. 17 (2017) 5817–5822.

[83] Y. Chen, S. Xu, S. Zhu, R.J. Jacob, G. Pastel, Y. Wang, Y. Li, J. Dai, F. Chen, H. Xie, B. Liu, Y. Yao, L.G. Salamanca-Riba, M.R. Zachariah, T. Li, L. Hu, Millisecond synthesis of CoS nanoparticles for highly efficient overall water splitting, Nano Res. 12 (2019) 2259–2267.

[84] M. Cui, C. Yang, B. Li, Q. Dong, M. Wu, S. Hwang, H. Xie, X. Wang, G. Wang, L. Hu, High-entropy metal sulfide nanoparticles promise high-performance oxygen evolution reaction, Adv. Energy Mater. 11 (2020), 2002887.

[85] Q. Dong, M. Hong, J. Gao, T. Li, M. Cui, S. Li, H. Qiao, A.H. Brozena, Y. Yao, X. Wang, G. Chen, J. Luo, L. Hu, Rapid synthesis of high-entropy oxide microparticles, Small 18 (2022), 2104761.

[86] W. Peng, Y. Feng, X. Yan, F. Hou, L. Wang, J. Liang, Multiatom catalysts for energy-related electrocatalysis, Adv. Sustain. Syst. 5 (2020), 2000213.

[87] M. Fang, G. Dong, R. Wei, J.C. Ho, Hierarchical nanostructures: design for sustainable water splitting, Adv. Energy Mater. 7 (2017), 1700559.

[88] L. Xing, R. Liu, Z. Gong, J. Liu, J. Liu, H. Gong, K. Huang, H. Fei, Ultrafast Joule heating synthesis of hierarchically porous graphene-based Co-N-C single-atom monoliths, Nano Res. 15 (2021) 3913–3919.

[89] M. Luo, Z. Zhao, Y. Zhang, Y. Sun, Y. Xing, F. Lv, Y. Yang, X. Zhang, S. Hwang, Y. Qin, J.Y. Ma, F. Lin, D. Su, G. Lu, S. Guo, PdMo bimetallene for oxygen reduction catalysis, Nature 574 (2019) 81–85.

[90] R. Chattot, O. Le Bacq, V. Beermann, S. Kuhl, J. Herranz, S. Henning, L. Kuhn, T. Asset, L. Guetaz, G. Renou, J. Drnec, P. Bordet, A. Pasturel, A. Eychmuller, T. J. Schmidt, P. Strasser, L. Dubau, F. Maillard, Surface distortion as a unifying concept and descriptor in oxygen reduction reaction electrocatalysis, Nat. Mater. 17 (2018) 827–833.

[91] L. Bu, N. Zhang, S. Guo, X. Zhang, J. Li, J. Yao, T. Wu, G. Lu, J. Ma, D. Su, X. Huang, Biaxially strained PtPb/Pt core/shell nanoplate boosts oxygen reduction catalysis, Science 354 (2016) 1410–1414.

[92] S. Liu, Y. Shen, Y. Zhang, B. Cui, S. Xi, J. Zhang, L. Xu, S. Zhu, Y. Chen, Y. Deng, W. Hu, Extreme environmental thermal shock induced dislocation-rich Pt nanoparticles boosting hydrogen evolution reaction, Adv. Mater. 34 (2022), 2106973.

[93] C. Kavakli, S. Meini, G. Harzer, N. Tsiouvaras, M. Piana, A. Siebel, A. Garsuch, H. A. Gasteiger, J. Herranz, Nanosized carbon-supported manganese oxide phases as lithium-oxygen battery cathode catalysts, ChemCatChem 5 (2013) 3358–3373.

[94] J. Xu, J. Li, D. Xiong, B. Zhang, Y. Liu, K.H. Wu, I. Amorim, W. Li, L. Liu, Trends in activity for the oxygen evolution reaction on transition metal (M = Fe, Co, Ni) phosphide pre-catalysts, Chem. Sci. 9 (2018) 3470–3476.

[95] D. Wang, T. Sheng, J. Chen, H. Wang, P. Hu, Identifying the key obstacle in photocatalytic oxygen evolution on rutile TiO_2, Nat. Catal. 1 (2018) 291–299.

[96] K. Liu, C. Zhang, Y. Sun, G. Zhang, X. Shen, F. Zou, H. Zhang, Z. Wu, E. C. Wegener, C.J. Taubert, J.T. Miller, Z. Peng, Y. Zhu, High-performance transition metal phosphide alloy catalyst for oxygen evolution reaction, ACS Nano 12 (2018) 158–167.

[97] J. Yu, Q. Li, Y. Li, C. Xu, L. Zhen, V.P. Dravid, J. Wu, Ternary metal phosphide with triple-layered structure as a low-cost and efficient electrocatalyst for bifunctional water splitting, Adv. Funct. Mater. 26 (2016) 7644–7651.

[98] L.-A. Stern, L. Feng, F. Song, X. Hu, Ni_2P as a Janus catalyst for water splitting: the oxygen evolution activity of Ni_2P nanoparticles, Energy Environ. Sci. 8 (2015) 2347–2351.

[99] L.M. Cao, Y.W. Hu, S.F. Tang, A. Iljin, J.W. Wang, Z.M. Zhang, T.B. Lu, Fe-CoP electrocatalyst derived from a bimetallic prussian blue analogue for large-current-density oxygen evolution and overall water splitting, Adv. Sci. 5 (2018), 1800949.

[100] A. Abdelhafiz, B. Wang, A.R. Harutyunyan, J. Li, Carbothermal shock synthesis of high entropy oxide catalysts: dynamic structural and chemical reconstruction boosting the catalytic activity and stability toward oxygen evolution reaction, Adv. Energy Mater. 12 (2022), 2200742.

[101] M. Chu, C. Chen, Y. Wu, X. Yan, S. Jia, R. Feng, H. Wu, M. He, B. Han, Enhanced CO_2 electroreduction to ethylene via strong metal-support interaction, Green. Energy Environ. 7 (2022) 792–798.

[102] W. Ren, X. Tan, W. Yang, C. Jia, S. Xu, K. Wang, S.C. Smith, C. Zhao, Isolated diatomic Ni-Fe metal-nitrogen sites for synergistic electroreduction of CO_2, Angew. Chem. Int. Ed. 58 (2019) 6972–6976.

[103] B. Chang, H. Pang, F. Raziq, S. Wang, K. Huang, J. Ye, H. Zhang, Electrochemical reduction of carbon dioxide to multicarbon (C_{2+}) products: challenges and perspectives, Energy Environ. Sci. (2023), https://doi.org/10.1039/D1033EE00964E.

[104] D. Yang, B. Ni, X. Wang, Heterogeneous catalysts with well-defined active metal sites toward CO_2 electrocatalytic reduction, Adv. Energy Mater. 10 (2020), 2001142.

[105] X. Wang, Z. Chen, X. Zhao, T. Yao, W. Chen, R. You, C. Zhao, G. Wu, J. Wang, W. Huang, J. Yang, X. Hong, S. Wei, Y. Wu, Y. Li, Regulation of coordination number over single Co sites: triggering the efficient electroreduction of CO_2, Angew. Chem. Int. Ed. 57 (2018) 1944–1948.

[106] J. Yang, W. Li, D. Wang, Y. Li, Single-atom materials: small structures determine macroproperties, Small Struct. 2 (2020), 2000051.

[107] D. Xi, J. Li, J. Low, K. Mao, R. Long, J. Li, Z. Dai, T. Shao, Y. Zhong, Y. Li, Z. Li, X. J. Loh, L. Song, E. Ye, Y. Xiong, Limiting the uncoordinated N species in $M-N_x$ single-atom catalysts toward electrocatalytic CO_2 reduction in broad voltage range, Adv. Mater. 34 (2022), 2104090.

[108] B. Chang, L. Li, D. Shi, H. Jiang, Z. Ai, S. Wang, Y. Shao, J. Shen, Y. Wu, Y. Li, X. Hao, Metal-free boron carbonitride with tunable boron Lewis acid sites for enhanced nitrogen electroreduction to ammonia, Appl. Catal. B: Environ. 283 (2021), 119622.

[109] B. Chang, H. Yuan, L. Li, J. Yu, X. Liu, W. Yu, B. Wang, L. Zhao, S. Liu, S. Sun, H. Liu, W. Zhou, Enhancing electrochemical nitrogen fixation by mimicking π back-donation on laser-tuned Lewis acid sites in noble-metal-molybdenum carbide, Appl. Catal. B: Environ. 320 (2023), 121777.

[110] C. Kim, J.Y. Song, C. Choi, J.P. Ha, W. Lee, Y.T. Nam, D.M. Lee, G. Kim, I. Gereige, W.B. Jung, H. Lee, Y. Jung, H. Jeong, H.T. Jung, Atomic-scale homogeneous Ru-Cu alloy nanoparticles for highly efficient electrocatalytic nitrogen reduction, Adv. Mater. 34 (2022), 2205270.

[111] M. Wu, Z. Zhou, Covalent organic frameworks as electrode materials for rechargeable metal-ion batteries, Interdisciplinary. Materials 2 (2023) 231–259.

[112] Y. Lv, L. Zhang, X. Wei, B. Qiu, W. Zhang, Q. Qin, D. Jia, X. He, Z. Liu, F. Wei, The emerging of zinc-ion hybrid supercapacitors: advances, challenges, and future perspectives, Sustain. Mater. Technol. 35 (2023) 00536.

[113] J. Zhang, J. Luo, Z. Guo, Z. Liu, C. Duan, S. Dou, Q. Yuan, P. Liu, K. Ji, C. Zeng, J. Xu, W. Liu, Y. Chen, W. Hu, Ultrafast manufacturing of ultrafine structure to achieve an energy density of over 120 Wh kg^{-1} in supercapacitors, Adv. Energy Mater. 13 (2022), 2203061.

[114] A. Manthiram, X. Yu, S. Wang, Lithium battery chemistries enabled by solid-state electrolytes, Nat. Rev. Mater. 2 (2017) 16103.

[115] L.J. Miara, W.D. Richards, Y.E. Wang, G. Ceder, First-principles studies on cation dopants and electrolyte cathode interphases for lithium garnets, Chem. Mater. 27 (2015) 4040–4047.

[116] J. van den Broek, S. Afyon, J.L.M. Rupp, Interface-engineered all-solid-state Li-ion batteries based on garnet-type fast Li^+ conductors, Adv. Energy Mater. 6 (2016), 1600736.

[117] B. Liu, K. Fu, Y. Gong, C. Yang, Y. Yao, Y. Wang, C. Wang, Y. Kuang, G. Pastel, H. Xie, E.D. Wachsman, L. Hu, Rapid thermal annealing of cathode-garnet interface toward high-temperature solid state batteries, Nano Lett. 17 (2017) 4917–4923.

[118] W.D. Richards, L.J. Miara, Y. Wang, J.C. Kim, G. Ceder, Interface stability in solid-state batteries, Chem. Mater. 28 (2015) 266–273.

[119] A. Sharafi, S. Yu, M. Naguib, M. Lee, C. Ma, H.M. Meyer, J. Nanda, M. Chi, D. J. Siegel, J. Sakamoto, Impact of air exposure and surface chemistry on $Li–Li_7La_3Zr_2O_{12}$ interfacial resistance, J. Mater. Chem. A 5 (2017) 13475–13487.

[120] C. Wang, H. Xie, W. Ping, J. Dai, G. Feng, Y. Yao, S. He, J. Weaver, H. Wang, K. Gaskell, L. Hu, A general, highly efficient, high temperature thermal pulse toward high performance solid state electrolyte, Energy Storage Mater. 17 (2019) 234–241.

[121] Y. Liu, S. Shrestha, W.E. Mustain, Synthesis of nanosize tungsten oxide and its evaluation as an electrocatalyst support for oxygen reduction in acid media, ACS Catal. 2 (2012) 456–463.

[122] M.W. Glasscott, A.D. Pendergast, S. Goines, A.R. Bishop, A.T. Hoang, C. Renault, J.E. Dick, Electrosynthesis of high-entropy metallic glass nanoparticles for designer, multi-functional electrocatalysis, Nat. Commun. 10 (2019) 2650.

[123] J. Lu, S. Liu, J. Liu, G. Qian, D. Wang, X. Gong, Y. Deng, Y. Chen, Z. Wang, Millisecond conversion of photovoltaic silicon waste to binder-free high silicon content nanowires electrodes, Adv. Energy Mater. 11 (2021), 2102103.

[124] W. Zhu, J. Zhang, J. Luo, C. Zeng, H. Su, J. Zhang, R. Liu, E. Hu, Y. Liu, W.D. Liu, Y. Chen, W. Hu, Y. Xu, Ultrafast non-equilibrium synthesis of cathode materials for Li-ion batteries, Adv. Mater. 35 (2023), 2208974.

[125] P.G. Bruce, S.A. Freunberger, L.J. Hardwick, J.M. Tarascon, Li-O_2 and Li-S batteries with high energy storage, Nat. Mater. 11 (2011) 19–29.

[126] W.B. Jung, H. Park, J.S. Jang, D.Y. Kim, D.W. Kim, E. Lim, J.Y. Kim, S. Choi, J. Suk, Y. Kang, I.D. Kim, J. Kim, M. Wu, H.T. Jung, Polyelemental nanoparticles as catalysts for a Li-O_2 battery, ACS Nano 15 (2021) 4235–4244.

[127] M. Armand, J.M. Tarascon, Building better batteries, Nature 451 (2008) 652–657.

[128] G. Li, Y. Mu, Z. Huang, N. Wang, Y. Chen, J. Liu, G. Liu, O.L. Li, M. Shao, Z. Shi, Poly-active centric Co_3O_4-CeO_2/Co-N-C composites as superior oxygen reduction catalysts for Zn-air batteries, Sci. China Mater. 64 (2020) 73–84.

[129] J. Wang, K. Wang, F.B. Wang, X.H. Xia, Bioinspired copper catalyst effective for both reduction and evolution of oxygen, Nat. Commun. 5 (2014) 5285.

[130] J. Wang, F. Xu, H. Jin, Y. Chen, Y. Wang, Non-noble metal-based carbon composites in hydrogen evolution reaction: fundamentals to applications, Adv. Mater. 29 (2017), 1605838.

[131] Q. Lu, H. Wu, X. Zheng, Y. Chen, A.L. Rogach, X. Han, Y. Deng, W. Hu, Encapsulating cobalt nanoparticles in interconnected N-doped hollow carbon nanofibers with enriched Co-N-C moiety for enhanced oxygen electrocatalysis in Zn-air batteries, Adv. Sci. 8 (2021), 2101438.
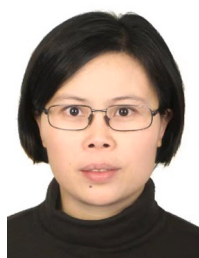
[132] X. Li, F. Chen, B. Zhao, S. Zhang, X. Zheng, Y. Wang, X. Jin, C. Dai, J. Wang, J. Xie, Z. Zhang, Y. Zhao, Ultrafast synthesis of metal-layered hydroxides in a dozen seconds for high-performance aqueous Zn (micro-) battery, Nano-Micro Lett. 15 (2023) 32.

[133] Y. Li, H. Wu, J. Zhang, Q. Lu, X. Han, X. Zheng, Y. Deng, W. Hu, Rapid synthesis of doped metal oxides via Joule heating for oxygen electrocatalysis regulation, J. Mater. Chem. A 11 (2023) 10267–10276.

[134] Z. Xie, X. Zhang, Z. Zhang, Z. Zhou, Metal-CO_2 batteries on the road: CO_2 from contamination gas to energy source, Adv. Mater. 29 (2017), 1605891.

[135] C. Li, Z. Guo, B. Yang, Y. Liu, Y. Wang, Y. Xia, A rechargeable Li-CO_2 battery with a gel polymer electrolyte, Angew. Chem. Int. Ed. 56 (2017) 9126–9130.

[136] X. Hu, Z. Li, J. Chen, Flexible Li-CO_2 batteries with liquid-free electrolyte, Angew. Chem. Int. Ed. 56 (2017) 5785–5789.

[137] T.S. Wei, B.Y. Ahn, J. Grotto, J.A. Lewis, 3D printing of customized Li-ion batteries with thick electrodes, Adv. Mater. 30 (2018), 1703027.

[138] Y. Qiao, S. Xu, Y. Liu, J. Dai, H. Xie, Y. Yao, X. Mu, C. Chen, D.J. Kline, E.M. Hitz, B. Liu, J. Song, P. He, M.R. Zachariah, L. Hu, Transient, in situ synthesis of ultrafine ruthenium nanoparticles for a high-rate Li-CO_2 battery, Energy Environ. Sci. 12 (2019) 1100–1107.

Lianbo Ma received his Ph.D. in Physical Chemistry from Nanjing University. Then, he got a postdoc position sponsored by the Hong Kong Innovation and Technology Fund (ITF), and worked at The Hong Kong University of Science and Technology (HKUST). In October 2019, he joined the School of Materials Science and Engineering at Anhui University of Technology. His research mainly includes the development of novel micro-and nanostructured materials for secondary batteries, and the exploration of integrated energy conversion and storage systems.

Wei Zhang received her Ph.D. degree at Anhui University of Technology in 2021. Now, she is a senior engineer at the School of Materials Science and Engineering, Anhui University of Technology, China. Her research interest focuses on the synthesis of carbon-based materials for energy conversion and storage.
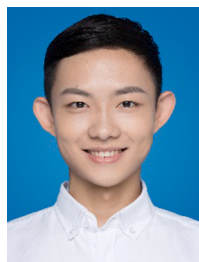
Yaohui Lv received his Ph.D. degree at Shandong University in 2010. Now, he is a associate professor at the School of Materials Science and Engineering, Anhui University of Technology, China. His research interest is related to the design and synthesis of carbon-based materials and devices for new energy conversion and storage, including Na-ion battery and supercapacitor.

Xiang Wei received his B.S. from Anhui University of Technology, and he is now pursuing his M.S. in materials science at Anhui University of Technology, under the supervision of Yaohui Lv. His research mainly focuses on new materials for Na-ion batteries.

Prof. Weijia Zhou completed his Ph.D. at Shandong University in 2012. Now, Dr. Zhou is a professor in the Institute for Advanced Interdisciplinary Research (IAIR), University of Jinan (UJN), Shandong. His research interests are related to the design and synthesis of functional materials and devices for clean energy conversion and circulation, including photo and electro-catalytic water splitting, CO_2 reduction.

Tong Wu obtained his M.S. degree from University of Jinan in 2020. Currently, he studies as a doctor student in Prof. Weijia Zhou's team in the Institute for Advanced Interdisciplinary Research (IAIR), University of Jinan. His current research focus on laser-catalysis system, including ammonia synthesis and CO_2 conversion.

Prof. Hong Liu is a professor in State Key Laboratory of Crystal Materials, Shandong University. He received his Ph.D. degree in 2001 from Shandong University (China). His current research is mainly focused on chemical processing of nanomaterials for energy related applications including photocatalysis, tissue engineering, especially the interaction between stem cell and nanostructure of biomaterials as well as the nonlinear optical crystals.

FengWei received his Ph.D. in Materials Science and Engineering from Anhui University of Technology in 2020. Then, he joined the School of Materials and Chemical Engineering at Chuzhou University. His research interests mainly include the preparation of carbon materials and their application in batteries, supercapacitors and hybrid capacitors.